Supporting Information
For

Effect of ligand substituents on the reactivity conduits of copper (II) complexes towards electrocatalytic water oxidation

Hemrupa Kuilya,[a] Pranjal Das,[a] Swati Basak,[a] Debajit Sarma,[b] Pradyumna Mazumdar,[a] Diganta Choudhury *,[a] and Apurba Kalita *,[a]

[a]*Department of Chemistry, B. Borooah College, Guwahati, Assam 781007, India*
[b]*Department of Chemistry, Indian Institute of Technology Patna, Patna 801103, Bihar, India*

Table of Contents:

Sl. No.	Contents	Page
1	**Experimental Procedures**	**7-8**
2	**Figure S1.** UV-visible spectrum of $\mathbf{L_1H}$ in methanol	**9**
3	**Figure S2.** FT-IR spectrum of $\mathbf{L_1H}$ in KBr	**9**
4	**Figure S3**ESI-Mass spectrum of the $\mathbf{L_1H}$ in methanol	**9**
5	**Figure S4** ^{1}H-NMR of $\mathbf{L_1H}$ in $CDCl_3$	**10**
6	**Figure S5** ^{13}C-NMR of $\mathbf{L_1H}$ in $CDCl_3$	**10**
7	**Figure S6.** UV-visible spectrum of ligand $\mathbf{L_3H}$ in methanol	**10**
8	**Figure S7.** FT-IR spectrum of $\mathbf{L_3H}$ in KBr.	**11**
9	**Figure S8.** ^{1}H-NMR of $\mathbf{L_3H}$ in CD_3OD	**11**
10	**Figure S9.** ^{13}C-NMR of $\mathbf{L_3H}$ in CD_3OD	**11**
11	**Figure S10.** UV-visible spectrum of complex **1** in methanol. The inset shows a magnified view of the 400-1000 nm region.	**12**
12	**Figure S11.** UV-visible spectrum of complex **1** in pH 7 buffer. The inset shows a magnified view of the 400-1000 nm region.	**12**
13	**Figure. S12.**FT-IR spectrum of complex **1**in KBr.	**12**
14	**Figure .S13.** UV-visible spectrum of complex**3**in methanol. The inset shows a magnified view of the 400-1000 nm region.	**13**
15	**Figure S14.** FT-IR spectrum of complex **3** in KBr.	**13**
16	**Figure S15.** PXRD pattern of complex **3**	**13**
17	**Figure S16.** Plot of i_p vs. $\upsilon^{1/2}$for the Cu^{II}/ Cu^{I} couple of complex**1**	**14**
18	**Figure S17.** Cyclic voltammogram of complex **1** at different scan rate. (black, red, green, navy blue, light blue, pink, yellow, dark yellow, dark blue, purple line at 10, 20, 30, 40, 50, 60, 70, 80, 90 and 100 mV/sec respectively)	**14**
19	**Figure S18.** Plot of i_p vs. $\upsilon^{1/2}$for the Cu^{II}/ Cu^{I} couple of complex **3**	**14**
20	**Figure S19.** Cyclic voltammogram of complex **3** at different scan rate (black, red, green, dark blue, light blue, magenta and yellow line at 80, 70, 60, 50, 40, 30 and 20 mV/sec respectively)	**15**
21	**Figure** S**20 (a**) Differential pulse voltammogram (DPV) of complex **1** in 0.1 M phosphate buffer at pH 6.07(black), 6.61(red), 7.01(green) and 7.41(dark blue). **(b)**Pourbaix diagram of complex **1** depicting change of potential of first (blck line), second (red line) and third (blue line) anodic peak with variation of pH of the buffer medium.	**15**
22	**Figure S21.(a**) Differential pulse voltammogram (DPV) of complex **2** in 0.1 M phosphate buffer at pH 7.0 (dark blue), 7.6 (green), 7.8 (red) and 8.0 (black). (b) Pourbaix diagram of complex **2** depicting change of potential of first (blck line), second (red line) and third (blue line) anodic peak with variation of pH of the buffer medium.	**16**

23	**Figure.S22** (a) Differential pulse voltammogram (DPV) of complex **3** in 0.1 M phosphate buffer at pH 6.8 (black), 7.4 (red), 7.6 (green) and 7.9 (blue). (b) Pourbaix diagram of complex **3** depicting change of potential of first (blck line), second (red line), third (blue line) and fourth (pink line) anodic peak with variation of pH of the buffer medium.	**16**
24	**Figure.S23** (**a**) Plot of E_{anode} (V vs. Ag/ AgCl) vs. ln νfor Cu^{II} /Cu^{I} couple (**b**) Plot of $E_{cathode}$(V vs. Ag/ AgCl) vs. ln ν for Cu^{II} /Cu^{I} couple **(c)**Plot of E_{anode} (V vs. Ag/ AgCl) vs. ln νfor Cu^{III} /Cu^{II}couple (**d**) Plot of $E_{cathode}$(V vs. Ag/ AgCl) vs. ln ν for Cu^{III} /Cu^{II} couple **(e)** Plot of $E_{a/2}$ (V vs. Ag/AgCl)vs. ln ν for third anodic peak **(f)**Plot of $E_{a/2}$ (V vs. Ag/AgCl)vs. ln ν for fourth anodic peak **(g)**Plot of $E_{a/2}$ (V vs. Ag/AgCl)vs. ln ν for fifth anodic peak for complex **1**.	**17**
25	**Figure S24.** (**a**) Plot of E_{anode} (V vs. Ag/ AgCl) vs. ln ν for Cu^{II} /Cu^{I} couple (**b**) Plot of $E_{cathode}$(V vs. Ag/ AgCl) vs. ln ν for Cu^{II} /Cu^{I} couple (c) Plot of $E_{a/2}$ (V vs. Ag/AgCl)vs. ln ν for second anodic peak (d) Plot of $E_{a/2}$ (V vs. Ag/AgCl)vs. ln ν for third anodic peak (e) Plot of $E_{a/2}$ (V vs. Ag/AgCl)vs. ln ν for fourth anodic peak of complex **2**.	**18**
26	**Figure S25.** (**a**) Plot of E_{anode} (V vs. Ag/ AgCl) vs. ln ν for Cu^{II} /Cu^{I} couple (**b**) Plot of $E_{cathode}$(V vs. Ag/AgCl) vs. ln ν for Cu^{II} /Cu^{I} couple (c) Plot of $E_{a/2}$ (V vs. Ag/AgCl)vs. ln ν for second anodic peak (d) Plot of $E_{a/2}$ (V vs. Ag/AgCl)vs. ln ν for third anodic peak (e) Plot of $E_{a/2}$ (V vs. Ag/AgCl)vs. ln ν for fourth anodic peak for complex **3**.	19
27	**Figure S26. (a)** UV-visible spectra of complex **1** after electrolysis at +0.76 V in neutral phosphate buffer at room temperature. **(b)** UV-visible spectra of complex **2** after electrolysis at +0.64V in neutral phosphate buffer at room temperature.**(c)** UV-visible spectra of complex **3** after electrolysis at +0.60 V in neutral phosphate buffer at room temperature.	**20**
28	**Figure S27.** Cyclic voltammogram of complex **1** (black) and analogous Zn^{2+}-complex (red) in neutral phosphate buffer at 100 mV s^{-1} scan rate	**20**
29	**Figure S28.** Cyclic voltammogram of complex **2** (black) and analogous Zn^{2+}-complex (red) in neutral phosphate buffer at 100 mV s^{-1} scan rate	**21**
30	**Figure S29.** Cyclic voltammogram of complex**3** (black) and analogous Zn^{2+}-complex (red) in neutral phosphate buffer at 100 mV s^{-1} scan rate.	**21**
31	**Figure S30.** Scan rate normalized CVof (a) complex **1**,(b) complex **2**and (**c**)complex **3**in 0.1 M neutral phosphate buffer.	**22**
32	**Figure S31. (Left)** Background corrected CV of complex**1** at 0.14(black), 0.22 (red), 0.26 (green), 0.30 (blue), 0.38 (cyan), 0.46 (magenta), 0.60mM(olive), concentration in 0.1 M neutral phosphate buffer. Scan rate: 100mV/s.**(Right)** Catalytic current at 1.51V as a function of the catalyst concentration from 0.14 to 0.60mM measured in 0.1 M neutral phosphate buffer.	**22**
33	**Figure S32.** Plot of current vs. concentration at +0.76V **(a)**, +0.89V **(c)**, +0.97V **(e)** and +1.08V **(g)**.Plot of current vs. square of concentration at +0.76V **(b)**, +0.89V **(d)**, +0.97V **(f)** and +1.08V **(h)** for complex **1**.	**23**
34	**Figure S33. (Left)** Background correctedCV of complex**3** at 0.04 (Black) 0.06 (red), 0.08(green), 0.10 (dark blue), 0.14 (light blue), 0.18 (magenta), 0.22 (yellow), 0.26 (dark yellow), 0.30 (orange), 0.34 (pink). 0.38 (wine), 0.42 (olive) mM concentration in 0.1 M neutral phosphate buffer. Scan rate: 100mV/s. **(Right)** Plot of catalytic current at 1.52 V against the concentration of the catalyst for complex **3**	**24**

35	**Figure S34.** Background corrected CV of complex **1** (a), complex (b) and complex **3** (c) recorded at 1mM concentration in 0.1 M neutral phosphate buffer at 100mV/sec scan rate. The current density of 1mA/cm^{2}was obtained at 1.51V, 1.49V and 1.52 V for complex **1**, **2** and **3**respectively.	**24**
36	**FigureS35** (a) to (d) FOWA for complex **1**. (e) Plot of the different k_{obs} values extracted from the foot-of-the-wave analysis at scan rate 90-200 mVs^{-1}. The black line represents the average k_{obs} value (~32 s^{-1}).	**25**
37	**Figure S36.** Foot-of-the-wave analysis plotting i_{cat}/i_d vs. $1/[1+\exp\{(F/RT)(E^o_{cat}-E)\}]$ at 90 (black), 120 (red), 180 (green) and 200 (dark blue) mVs^{-1} scan rates for complex **1**.	**26**
38	**Figure S37.** (a) to (e) FOWA. (f) Plot of the different kobs values extracted from the foot-of-the-wave analysis at scan rate 10-50 mVs^{-1} for complex **2**. In figure (f) the black line represents the average k_{obs} value (~100 s^{-1}).	**26**
39	**Figure S38**Foot-of-the-wave analysis plotting i_{cat}/i_d vs. $1/[1+\exp\{(F/RT)(E^o_{cat}-E)\}]$ at 10 (black), 15 (red), 20 (green), 30 (dark blue) and 50 (cyan) mVs^{-1} scan rates for complex **2**	**27**
40	**Figure S39.** (a) to (e) FOWA for complex **2.** (f) Plot of the different k_{obs} values extracted from the foot-of-the-wave analysis at scan rate 40-80 mVs^{-1} for complex **3**. The black line represents the average k_{obs} value (~248 s^{-1}).	27
41	**Figure S40.** Foot-of-the-wave analysis plotting i_{cat}/i_d vs. $1/[1+\exp\{(F/RT)(E^o_{cat}-E)\}]$ at 40 (black), 50 (red), 60 (green),70 (dark blue) and 80 (cyan) mVs^{-1} scan rates for complex **3**.	**28**
42	**Figure S41. (a)** Plot of charge vs. time recorded during bulk electrolysis of complex **1** at 0.1mM (black), 0.2mM (red), 0.3mM (green), 0.4mM (dark blue) and 0.5mM (light blue) concentration at 1.51 V vs. NHE in 0.1 M neutral phosphate buffer. (**b)** Plot of total charge vs. concentration of complex **1** after 1h of electrolysis	**28**
43	**Figure.S42 (a)** Plot of charge vs. time recorded during bulk electrolysis of complex **1** at 0.1mM (black), 0.2mM (red), 0.3mM (green), 0.4mM (dark blue) and 0.5mM (light blue) concentration at 1.49 V vs. NHE in 0.1 M neutral phosphate buffer. (**b)** Plot of total charge vs. concentration of complex **2** after 1h of electrolysis.	**28**
44	**Figure.S43 (a)** Plot of charge vs. time recorded during bulk electrolysis of complex **2** at 0.1mM (black), 0.2mM (red), 0.3mM (green), 0.4mM (dark blue) and 0.5mM (light blue) concentration at 1.52 V vs. NHE in 0.1 M neutral phosphate buffer. (**b)** Plot of total charge vs. concentration of complex **3** after 1h of electrolysis.	**29**
45	**Figure S44.** Plot of current density vs. time obtained frombulk electrolysis experiment with (blue line) and without (red line) complex **1**(a), complex **2** (b) and complex **3** (c) in 0.1 M neutral phosphate buffer using ITO working electrode (area 4 cm^2) at 1.51 V, 1.49 V and 1.52 V respectively	**29**
46	**Figure S45.**Plot of concentration of Oxygen evolved against time during bulk electrolysis experiment at 1.52 V versus NHE with complex **1** in0.1 M neutral phosphate buffer (red line). The black line indicates the theoretical amount of oxygen as assumed by charge passed with 100% faradaic efficiency.	**30**
47	**Figure S46.** Plot of concentration of Oxygen evolved against time during bulk electrolysis experiment at 1.49 V versus NHE with (blue line) and without (red line) complex **2** in0.1 M neutral phosphate buffer. The black line indicates the	**30**

	theoretical amount of oxygen as assumed by charge passed with 100% faradaic efficiency.	
48	**Figure S47.**Plot of concentration of Oxygen evolved against time during bulk electrolysis experiment at 1.52 V versus NHE with complex **3** in0.1 M neutral phosphate buffer (red line). The black line indicates the theoretical amount of oxygen as assumed by charge passed with 100% faradaic efficiency.	30
49	**Figure S48.** Cyclic voltammogram of complex 1**(a)**, complex **(b)** and complex **(c)**before (black) and after electrolysis (red) at 1.51 V, 1.49 V and 1.52 V vs NHE respectively for complex 1, complex 2 and complex 3 in 0.1 M neutral phosphate buffer	**31**
50	**Figure S49**. **(a)** UV-visible spectra of complex **1** before electrolysis (black), just after completion of electrolysis (red) and after 1h of completion of electrolysis (green) at 1.51 V vs. NHE in 0.1 M neutral phosphate buffer.**(b)** UV-visible spectra of complex **2** before electrolysis (blue), just after completion of electrolysis (green) and after 1h of completion of electrolysis (black) at 1.49 V vs. NHE in 0.1 M neutral phosphate buffer. **(c)** UV-visible spectra of complex **3** before electrolysis (blue), just after completion of electrolysis (green) and after 1h of completion of electrolysis (black) at 1.52 V vs. NHE in 0.1 M neutral phosphate buffer.	**32**
51	**Figure S50.** Cyclic voltammogram recorded in 0.1 M neutral phosphate buffer with fresh (black line) and used (red line) ITO working electrode (area 4 cm^2) for complex **1**	**33**
52	**Figure S51.** Cyclic voltammogram recorded in 0.1 M neutral phosphate buffer with fresh (black line) and used (red line) ITO working electrode (area 4 cm^2) for complex **2**	**33**
53	**Figure S52.** Cyclic voltammogram recorded in 0.1 M neutral phosphate buffer with fresh (black line) and used (red line) ITO working electrode (area 4 cm^2) for complex **3**.	**33**
54	**Figure S53.**FE-SEM and EDX plot of fresh ITO sample before electrolysis experiment of complex**1** in neutral phosphate buffer.	**34**
55	**FigureS54** FE-SEM and EDX plot of used ITO sample after electrolysis experiment of complex **1**in neutral phosphate buffer.	**35**
56	**Figure S55**FE-SEM and EDX plot of fresh ITO sample before electrolysis experiment of complex **2** in neutral phosphate buffer.	**36**
57	**Figure S56.** FE-SEM and EDX plot of used ITO sample after electrolysis experiment of complex **2** in neutral phosphate buffer.	**37**
58	**Figure S57.**FE-SEM and EDX plot of fresh ITO sample before electrolysis experiment of complex **3** in neutral phosphate buffer.	**38**
59	**Figure S58.**FE-SEM and EDX plot of used ITO sample after electrolysis experiment of complex **3** in neutral phosphate buffer.	**39**
60	**Figure S59.** DFT optimised structure of metal peroxo intermediates generated from (a Complex **1**, (b) Complex **2** and (c) Complex **3**).	**40**
61	**Figure S60.** UV-visible spectrum obtained from TDDFT calculations carried out on the DFT optimized structures of metal peroxo intermediates generated from complex **1** during its catalytic cycle. Peak at 358 nm is assigned for the electronic transition from HOMO-20 to LUMO.	**40**
62	**Figure S61.** UV-visible spectrum obtained from TDDFT calculations carried out on the DFT optimized structures of metal peroxo intermediates generated from complex 2 during its catalytic cycle. Peak at 385 nm is assigned for the	**41**

	electronic transition from HOMO-1 to LUMO.	
63	**Figure S62.** UV-visible spectrum obtained from TDDFT calculations carried out on the DFT optimized structures of metal peroxo intermediates generated from complex 3 during its catalytic cycle. Peak at 387 nm is assigned for the electronic transition from HOMO-1 to LUMO.	**41**
64	**Figure S63. (a)** Boundary surface diagram of HOMO-20 orbital calculated from the DFT optimized structure of the metal peroxo intermediated generated from complex **1** showing interaction between π* orbital of the peroxide ion with a d orbital of the metal center. **(b)** Boundary surface diagram of LUMO calculated from the DFT optimized structure of the metal peroxo intermediated generated from complex **1.**	**42**
65	**Figure S64. (a)** Boundary surface diagram of HOMO-1 orbital calculated from the DFT optimized structure of the metal peroxo intermediated generated from complex **2** showing interaction between π* orbital of the peroxide ion with a d orbital of the metal center. **(b)** Boundary surface diagram of LUMO calculated from the DFT optimized structure of the metal peroxo intermediated generated from complex 2**.**	**42**
66	**Figure S65. (a)** Boundary surface diagram of HOMO-1 orbital calculated from the DFT optimized structure of the metal peroxo intermediated generated from complex **3** showing interaction between π* orbital of the peroxide ion with a d orbital of the metal center. **(b)** Boundary surface diagram of LUMO calculated from the DFT optimized structure of the metal peroxo intermediated generated from complex **3.**	**43**
67	**Figure S66 (a)** UV-visible spectra of complex **1** before (black line) and after (red line) reaction with Cerric ammonium nitrate in aqueous medium. **(b)** UV-visible spectra of complex **2** before (black line) and after (red line) reaction with Cerric ammonium nitrate in aquous medium. **(c)** UV-visible spectra of complex **3** before (black line) and after (red line) reaction with Cerric ammonium nitrate in aqueous medium.	**43**
68	**Figure S67**. Plot of concentration of Oxygen evolved against time after addition of 10 ml degassed 1 mM aqueous solution of the metal complexes to 40 mL degassed 100 mM aqueous solution of Cerium ammonium nitrate (CAN) in a gas-tight cell equipped with magnetic stirring bar and calibrated Ocean Optics FOXY probe. The arrow corresponds to the point of addition of the complex solution.	**44**
69	**Table S1.**Total charge passed through working electrode after 1h of electrolysis of complex 1, 2 and 3 at the E_{cat} potential.	**44**
70	**Table S2.**Crystal data and structure refinement parameters for Complex **1**, **2** and **3**	**44**
71	**Table S3.**Coordinate file of the DFT optimized structure of metal oxo intermediate generated in the catalytic cycle of complex **3**.	**45**
72	**Table S4.**Coordinate file of the DFT optimized structure of metal peroxo intermediate generated in the catalytic cycle of complex **1**.	**46**
73	**Table S5.**Coordinate file of the DFT optimized structure of metal peroxo intermediate generated in the catalytic cycle of complex **2**.	**48**
74	**Table S6.**Coordinate file of the DFT optimized structure of metal peroxo intermediate generated in the catalytic cycle of complex **3**.	**49**
75	**Table S7.** TON calculated for complexes **1**, **2** and **3** for chemically driven water oxidation catalytic activity using Cerium ammonium nitrate (CAN).	**50**

Experimental Procedures:

All reagents and solvents were purchased from commercial sources and were of reagent grade. UV-visible spectra were recorded on Cary-60 UV-visible spectrophotometer. FT-IR spectra were recorded on a Cary 630 spectrophotometer with sample prepared as KBr pellets. ^{1}H-NMR spectra was obtained with a 400MHz Varian FT-spectrometer. Chemical shifts (δppm) were referenced either with an internal standard (Me_4Si) for organic compounds or to the residual solvent peaks. The magnetic moment of the complex were measured on a Cambridge magnetic balance. Conductivity measurements were recorded using a Eutech instrument CON 700. Electrochemical measurements were made using CHI 7035E bipotentiostat. Glassy carbon working electrode, Pt wire auxiliary electrode, and Ag/AgCl reference electrode were used in a three-electrode configuration. FE-SEM was recorded on a Zeiss microscope; SUPRA 55VP-Field Emission Scanning Electron Microscope. EDX was recorded on a Zeiss X-ray analyser; SUPRA 55VP-Field. The coating was done with Platinum before the experimental analysis. Powder XRD data were collected by using RigakuSmartlab X-ray diffractometer with Cu-Kα radiation (λ = 1.54056 Å), operating voltage of 40 kV and an operating current of 125 mA.

A suitable single crystal of each compound was carefully selected under a polarizing microscope and glued to a crystal mounting loop with paratone oil. The single crystal data were collected on a BRUKER AXS (D8 Quest System) X-ray diffractometer equipped with PHOTON 100 CMOS detector at 293(2) K. The X-ray generator was operated at 50 kV and 30 mA using Mo Kα (λ = 0.71073 Å) radiation. The unit cell measurement, data collection (φ and ω scan), integration, scaling and absorption corrections for the crystals of both complexes was done using Bruker Apex II software.[1]Data were collected with ω scan width of 0.5°. Sufficient numbers of frames were collected for different setting of φ keeping the sample-to-detector distance fixed. The data were reduced using SAINTPLUS,[2] and an empirical absorption correction was applied using the SADABS program.[3] The structure was solved and refined using SHELXL97[4] present in the WinGx suit of programs (Version 1.63.04a).[5] All the hydrogen positions were initially located in the difference Fourier maps, and for the final refinement, the hydrogen atoms were placed in geometrically ideal positions and refined in the riding mode. Final refinement included atomic positions for all the atoms, anisotropic thermal parameters for all the non-hydrogen atoms, and isotropic thermal parameters for all the hydrogen atoms. Full-matrix least-squares refinement against $|F^2|$ was carried out using the WinGx package of programs.[5]The hydrogen atoms of the coordinated and the lattice water were fixed using Olex2 1.2 package of programs.[6,7] Structural illustrations have been drawn with ORTEP-3 for Windows. Details of the structure solution and final refinements for the compounds are given in Table S2.CCDC: 2362016, 1879870 and 2285154 contains the crystallographic data for this paper. These data can be obtained free of charge from The Cambridge Crystallographic Data Center (CCDC) via www.ccdc.cam.ac.uk/data_request/cif.Structural illustrations have been drawn with ORTEP-3 for Windows.

Electron count in redox peak using Laviron equations:

To obtain the number of electrons transferred in a redox peak, Laviron equations are used. The Laviron equations are given as below.

$$E_{p,c} = E^{\Theta} - (RT/\alpha nF)\ln(\alpha nv/RTk) = C - (RT/\alpha nF)\ln(v) \quad (1)$$

$$E_{p,a} = E^{\Theta} + [RT/(1-\alpha)nF]\ln[(1-\alpha)nv/RTk] = C + [RT/(1-\alpha)nF]\ln(v) \quad (2)$$

$$E_{p/2} = C + [RT/(1-\alpha)nF]\ln(v) \quad (3)$$

Where, E^{Θ} is the standard potential, $E_{p,c}$is the potential for cathodic peak, $E_{p,a}$is the potential for anodic peak, R is the ideal gas constant, T is temperature, F is Faraday constant, k is the rate constant of the electrochemical reaction (s^{-1}) and C is the constant.

The α value is calculated using equation (1) and equation (2) for a reversible couple from the slope of $E_{p,a}$vs. ln ν and $E_{p,c}$ vs. ln ν. With the calculated value of α, number of electron (n)can be calculated. For the irreversible peak, number of electron (n) can be calculated using equation (3) from the slope of $E_{1/2}$ vs. ln ν. The value of $E_{p,a}$, $E_{p,c}$ and $E_{1/2}$ are obtained from the cyclic voltammograms of the complexes at different scan rates.

Calculation of Faradic efficiency

% Faradic efficiency = [(Actual amount of oxygen produced) /(Theoretically calculated amount of oxygen)] X 100

The theoretically calculated amount of oxygen during Bulk Electrolysis (BE) experiment can be obtained using the following relation:

Theoretical yield of oxygen (in ppm) = (QM / 4FV)

Where,

Q = Total charge passed during Bulk Electrolysis (BE) experiment in coulomb.

M = Molecular mass of oxygen in milligram

F = Faraday constant

V= Volume of the complex solution used for bulk electrolysis (BE) experiment in Litter

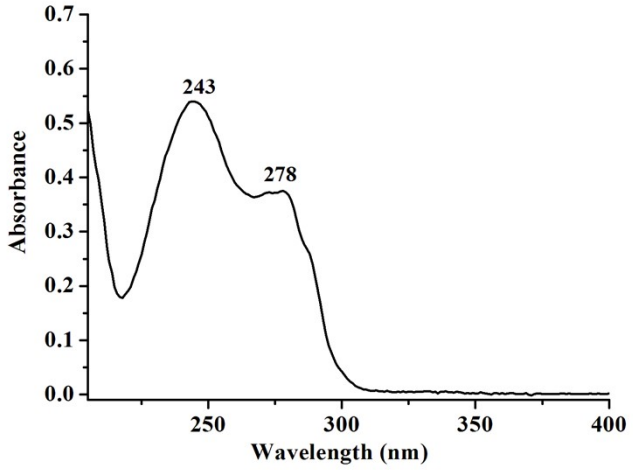

Figure S1. UV-visible spectrum of$\mathbf{L_1H}$ in methanol

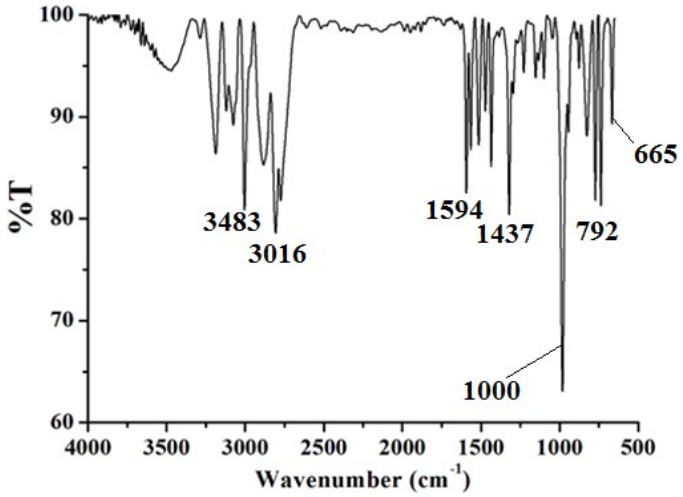

Figure S2FT-IR spectrum of $\mathbf{L_1H}$ in KBr.

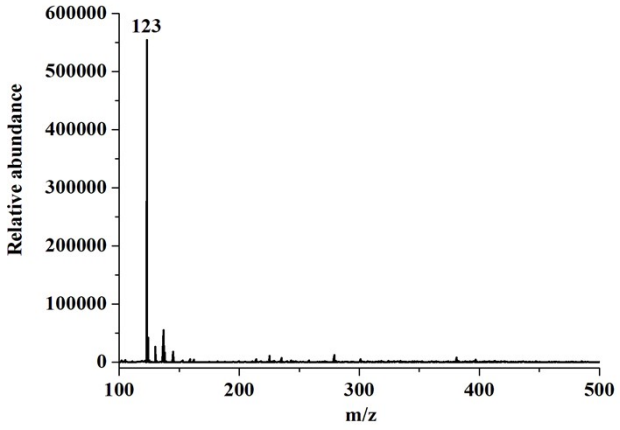

Figure S3ESI-Mass spectrum of the $\mathbf{L_1H}$ in methanol

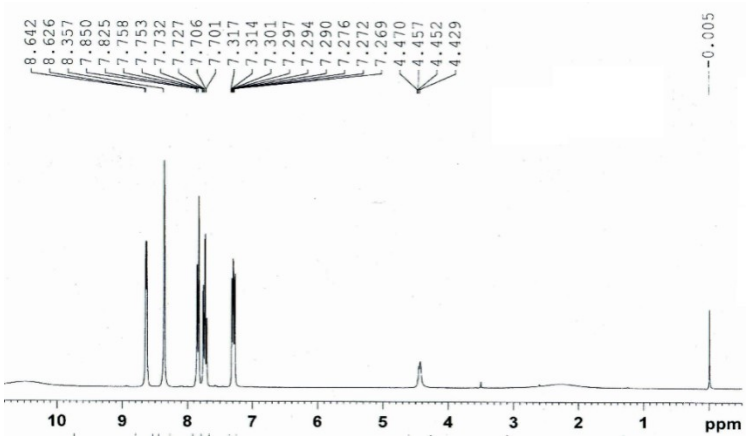

Figure S4^{1}H-NMR of $\mathbf{L_1H}$ in $CDCl_3$

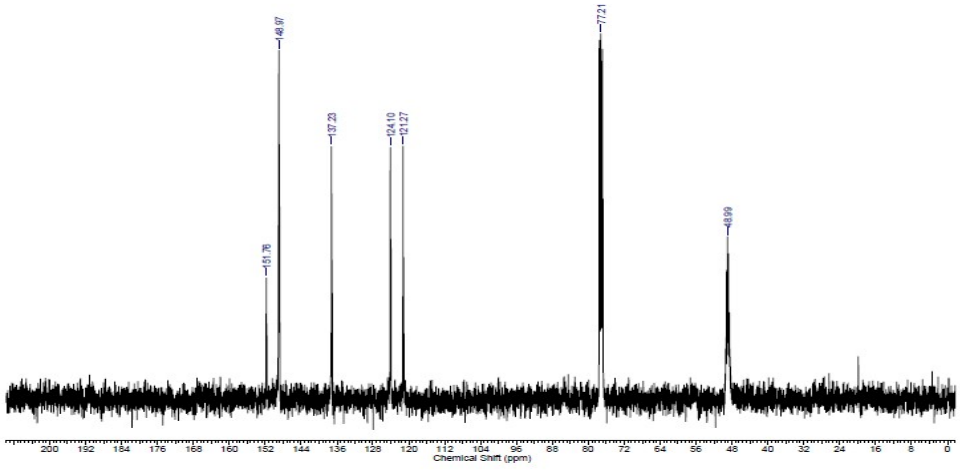

Figure S5^{13}C-NMR of $\mathbf{L_1H}$ in $CDCl_3$

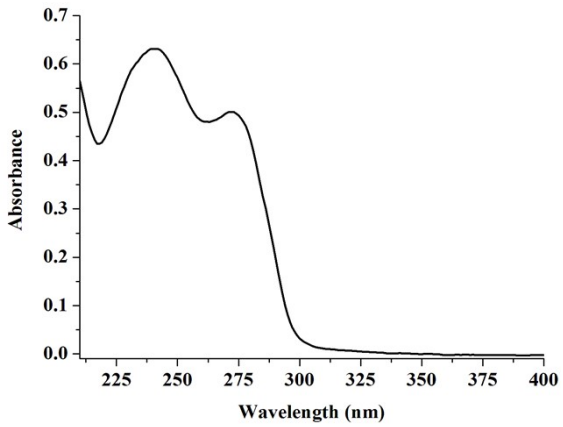

Figure S6. UV-visible spectrum of ligand $\mathbf{L_3H}$ in methanol

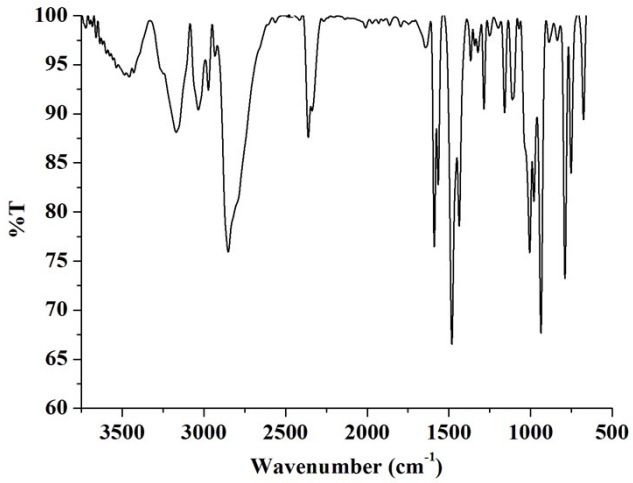

Figure S7. FT-IR spectrum of **L_3H** in KBr.

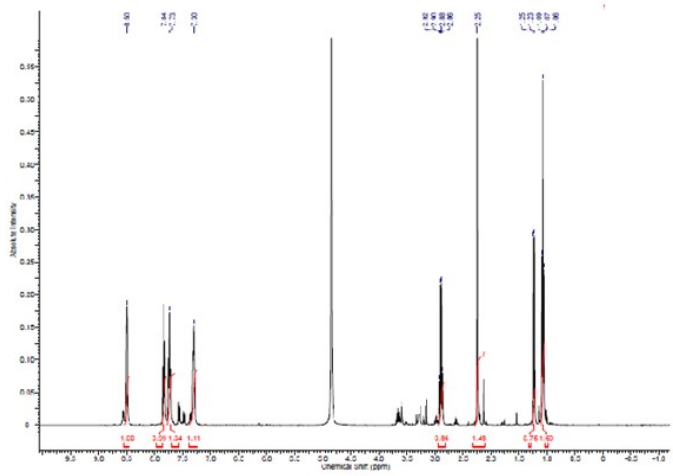

Figure S8. ^{1}H-NMR of **L_3H** in CD_3OD

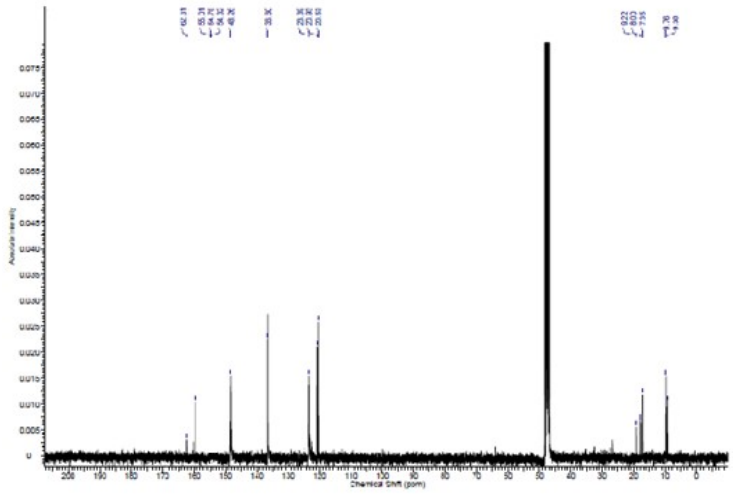

Figure S9. ^{13}C-NMR of **L_3H** in CD_3OD

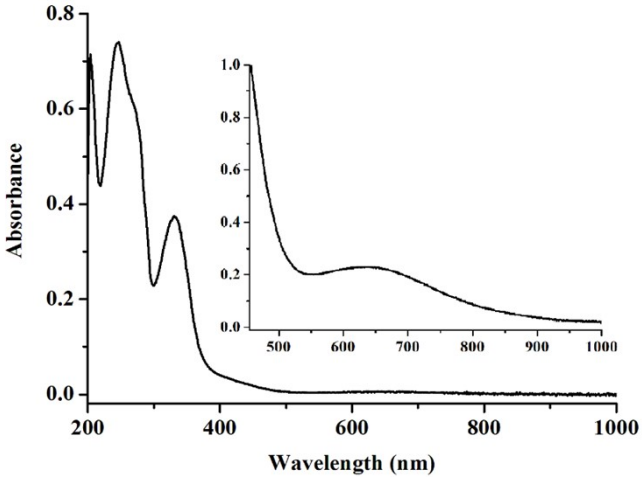

Figure S10.UV-visible spectrum of complex **1** in methanol. The inset shows a magnified view of the 400-1000 nm region.

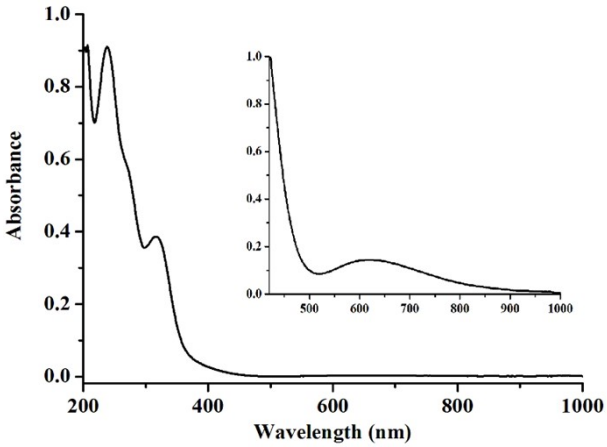

Figure S11.UV-visible spectrum of complex **1** in pH 7 buffer. The inset shows a magnified view of the 400-1000 nm region.

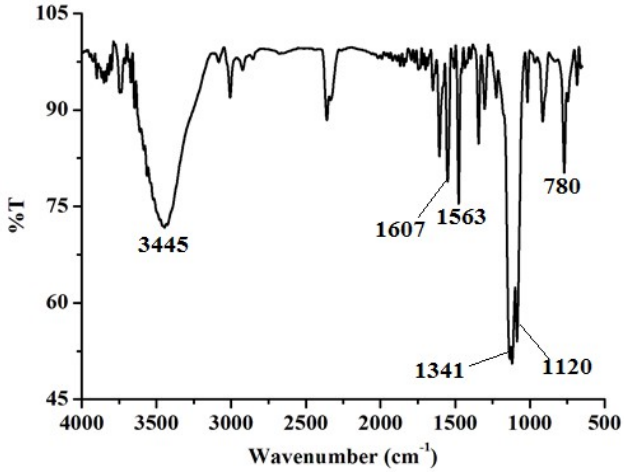

Figure.S12.FT-IR spectrum of complex **1**in KBr.

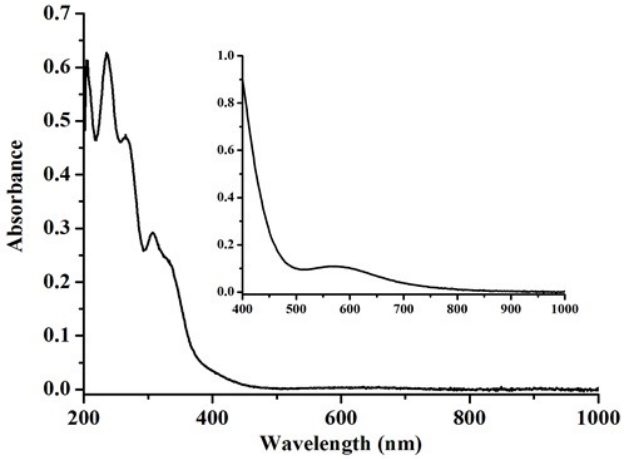

Figure .S13.UV-visible spectrum of complex**3**in methanol. The inset shows a magnified view of the 400-1000 nm region.

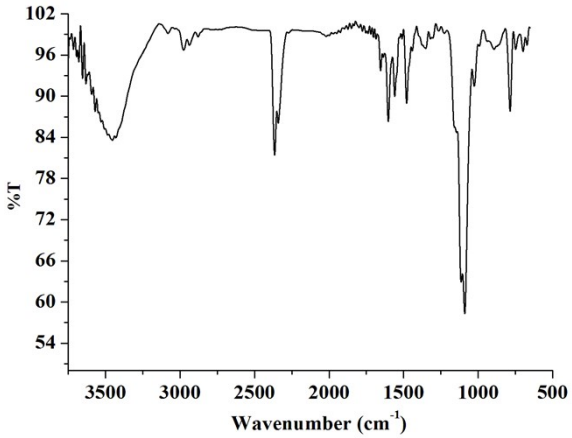

Figure S14. FT-IR spectrum of complex**3**in KBr.

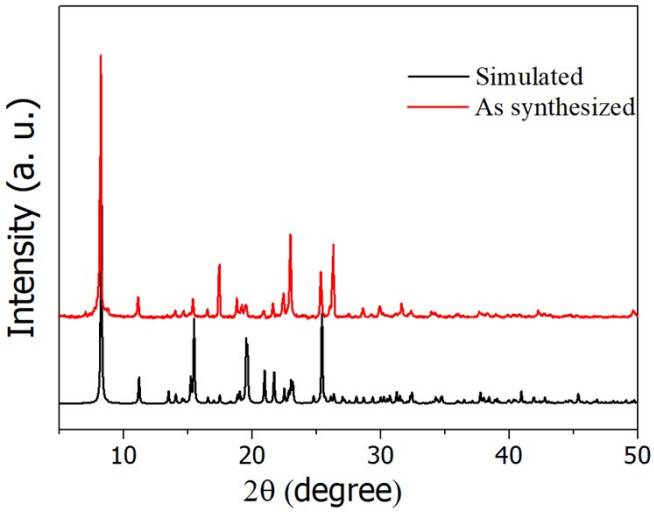

Figure S15. PXRD pattern of complex**3**

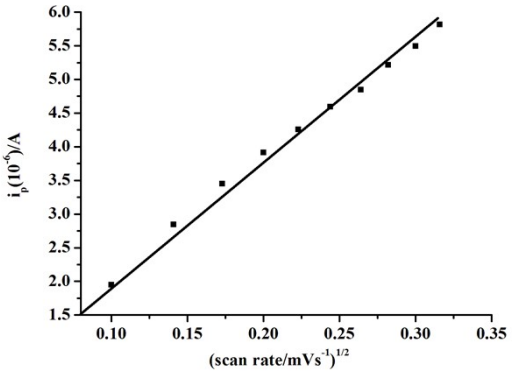

Figure S16. Plot of i_p vs. $\upsilon^{1/2}$for the Cu^{II}/ Cu^{I} couple of complex**1**

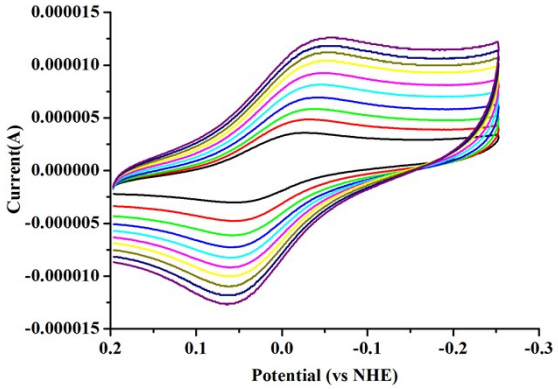

Figure S17. Cyclic voltammogram of complex **1** at different scan rate. (black, red, green, navy blue, light blue, pink, yellow, dark yellow, dark blue, purple line at 10, 20, 30, 40, 50, 60, 70, 80, 90 and 100 mV/sec respectively)

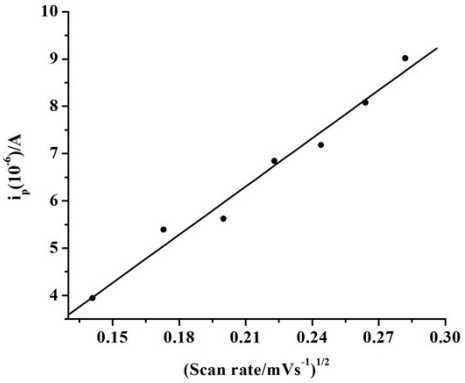

Figure S18. Plot of i_p vs. $\upsilon^{1/2}$for the Cu^{II}/ Cu^{I} couple of complex**3**

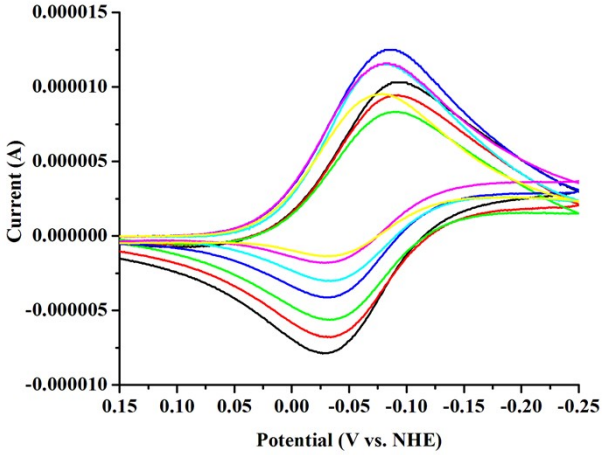

Figure S19. Cyclic voltammogram of complex **3** at different scan rate (black, red, green, dark blue, light blue, magenta and yellow line at 80, 70, 60, 50, 40, 30 and 20 mV/sec respectively)

(a) (b)

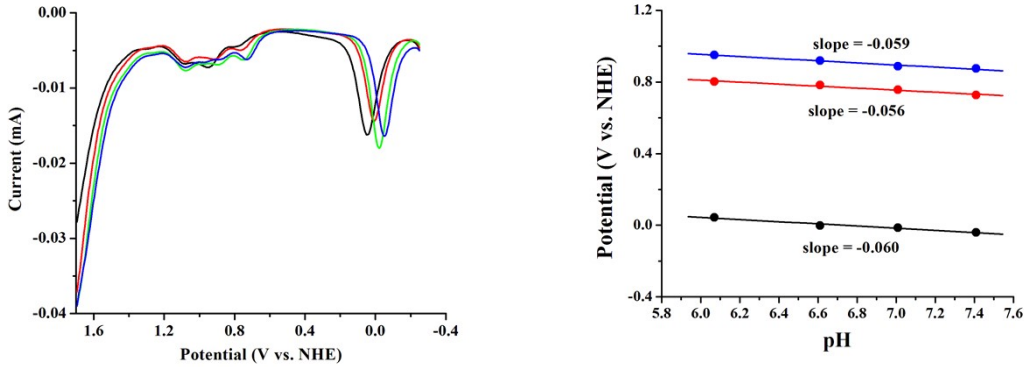

Figure S**20 (a**) Differential pulse voltammogram (DPV) of complex **1** in 0.1 M phosphate buffer at pH 6.07(black), 6.61(red), 7.01(green) and 7.41(dark blue). **(b)**Pourbaix diagram of complex **1** depicting change of potential of first (blck line), second (red line) and third (blue line) anodic peak with variation of pH of the buffer medium.

(a) (b)

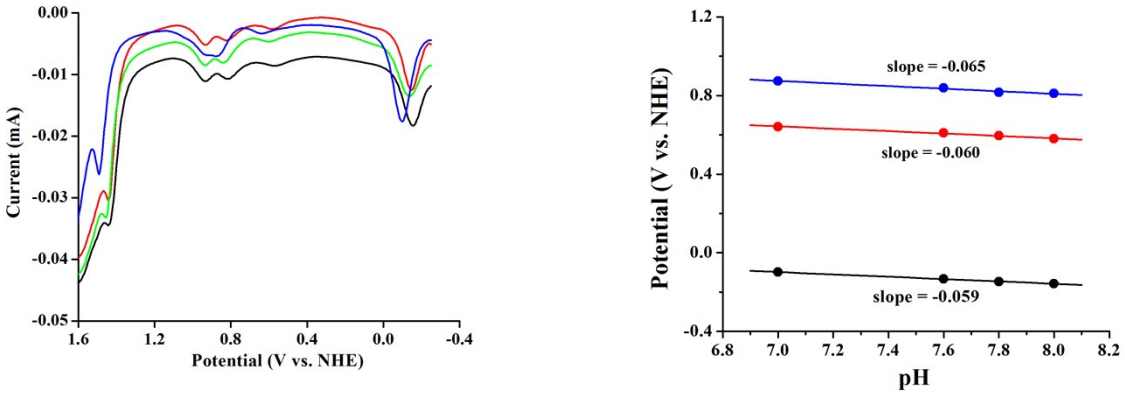

Figure S21.(a) Differential pulse voltammogram (DPV) of complex **2** in 0.1 M phosphate buffer at pH 7.0 (dark blue), 7.6 (green), 7.8 (red) and 8.0 (black). (b) Pourbaix diagram of complex **2** depicting change of potential of first (blck line), second (red line) and third (blue line) anodic peak with variation of pH of the buffer medium.

(a) (b)

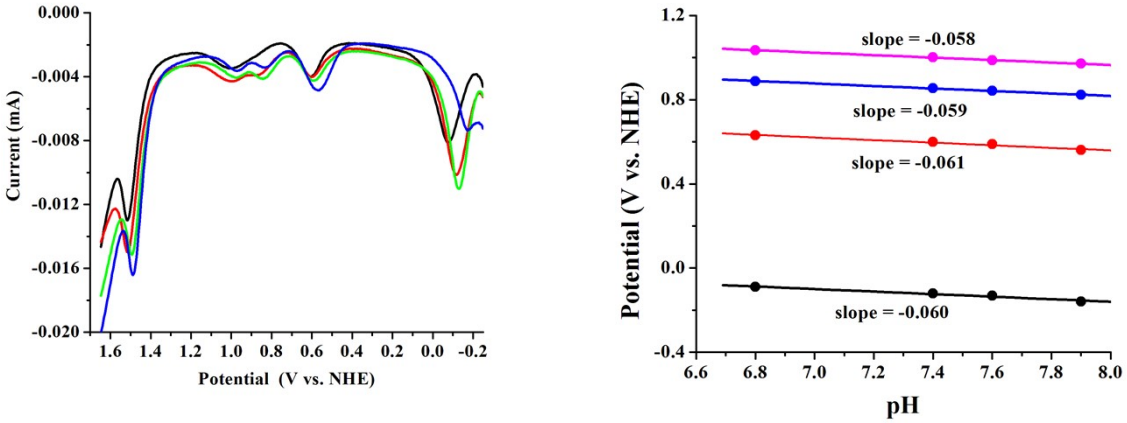

Figure.S22 (a) Differential pulse voltammogram (DPV) of complex **3** in 0.1 M phosphate buffer at pH 6.8 (black), 7.4 (red), 7.6 (green) and 7.9 (blue). (b) Pourbaix diagram of complex **3** depicting change of potential of first (blck line), second (red line), third (blue line) and fourth (pink line) anodic peak with variation of pH of the buffer medium.

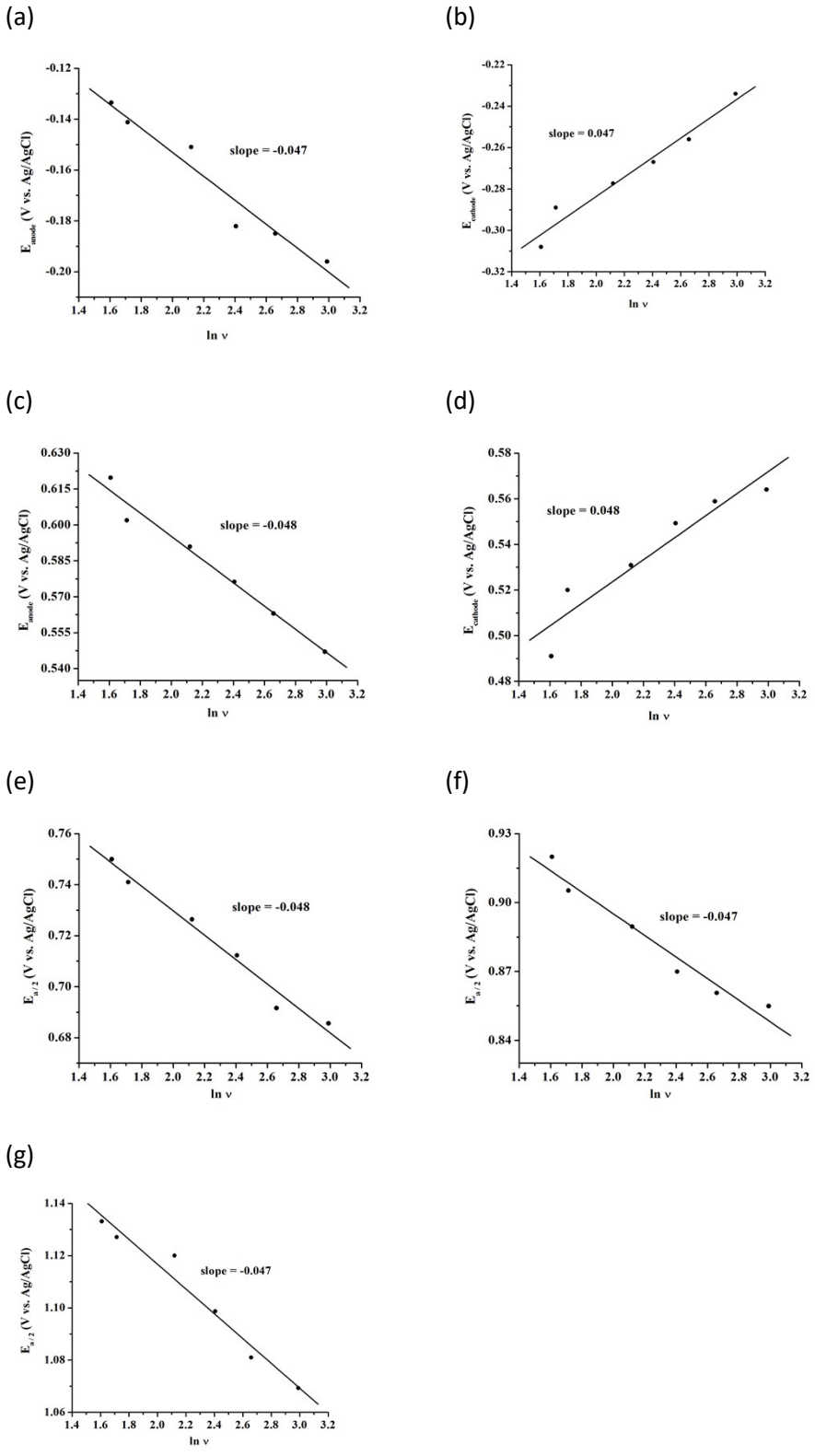

Figure.S23 (**a**) Plot of E_{anode} (V vs. Ag/ AgCl) vs. ln νfor Cu^{II} /Cu^{I} couple (**b**) Plot of $E_{cathode}$(V vs. Ag/ AgCl) vs. ln ν for Cu^{II} /Cu^{I} couple **(c)**Plot of E_{anode} (V vs. Ag/ AgCl) vs. ln νfor Cu^{III} /Cu^{II}couple (**d**) Plot of $E_{cathode}$(V vs. Ag/ AgCl) vs. ln ν for Cu^{III} /Cu^{II} couple **(e)** Plot of $E_{a/2}$ (V vs. Ag/AgCl)vs. ln ν for third anodic peak **(f)**Plot of $E_{a/2}$ (V vs. Ag/AgCl)vs. ln ν for fourth anodic peak **(g)**Plot of $E_{a/2}$ (V vs. Ag/AgCl)vs. ln ν for fifth anodic peak for complex **1**.

(a)

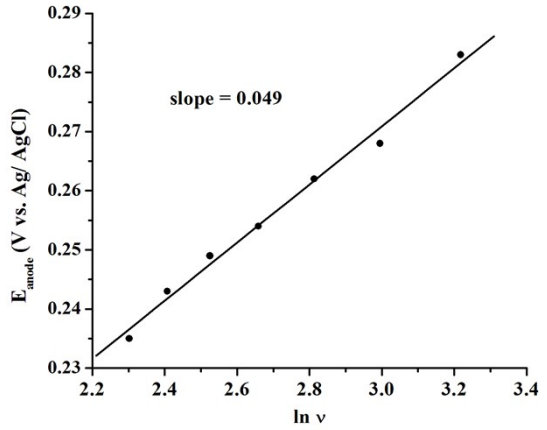

(b)

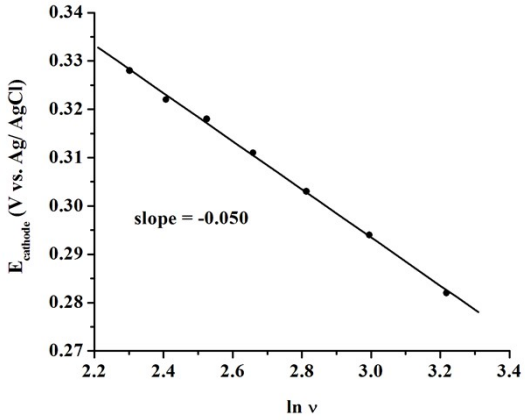

(c)

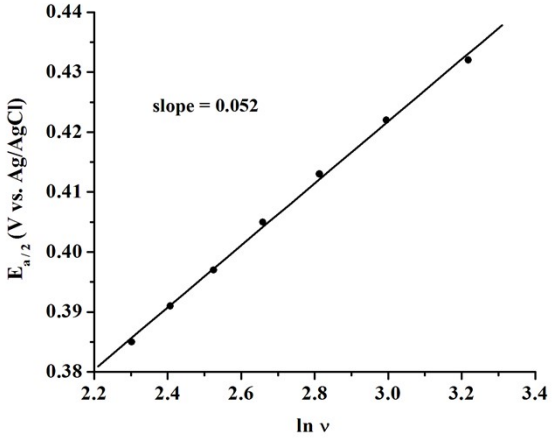

(d)

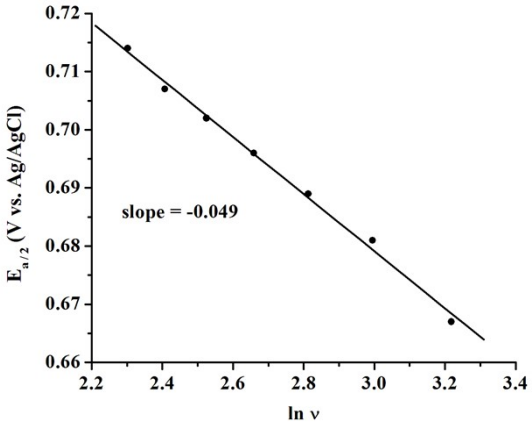

(e)

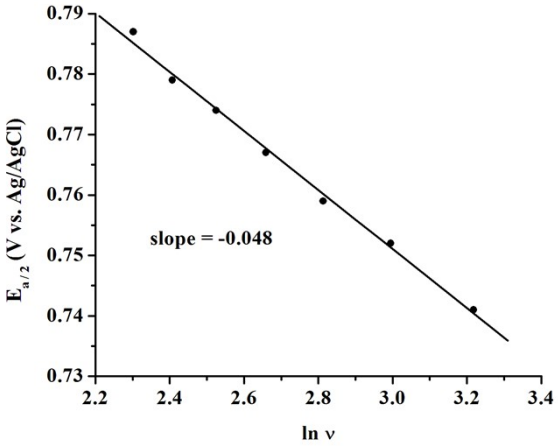

Figure S24. (**a**) Plot of E_{anode} (V vs. Ag/ AgCl) vs. ln ν for Cu^{II} /Cu^{I} couple (**b**) Plot of $E_{cathode}$(V vs. Ag/ AgCl) vs. ln ν for Cu^{II} /Cu^{I} couple (c) Plot of $E_{a/2}$ (V vs. Ag/AgCl)vs. ln ν for second anodic peak (d) Plot of $E_{a/2}$ (V vs. Ag/AgCl)vs. ln ν for third anodic peak (e) Plot of $E_{a/2}$ (V vs. Ag/AgCl)vs. ln ν for fourth anodic peak of complex **2**.

(a)

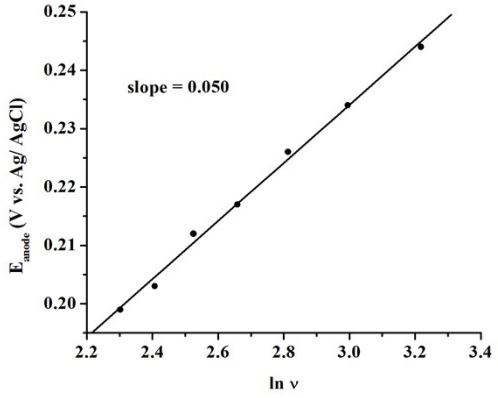

(b)

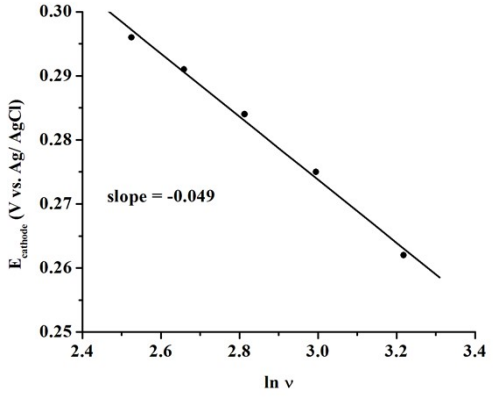

(c)

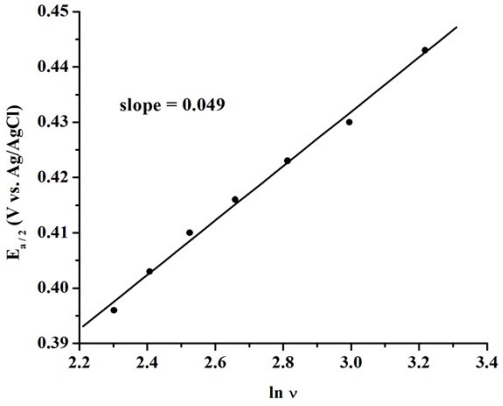

(d)

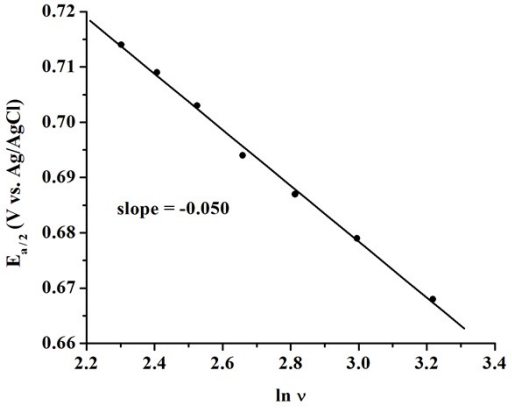

(e)

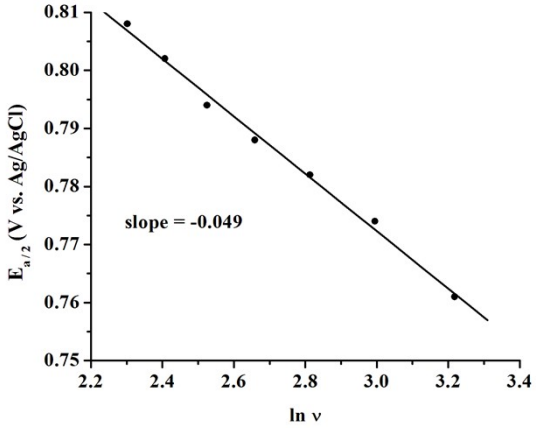

Figure S25. (**a**) Plot of E_{anode} (V vs. Ag/ AgCl) vs. ln ν for Cu^{II} /Cu^{I} couple (**b**) Plot of $E_{cathode}$(V vs. Ag/AgCl) vs. ln ν for Cu^{II} /Cu^{I} couple (c) Plot of $E_{a/2}$ (V vs. Ag/AgCl)vs. ln ν for second anodic peak (d) Plot of $E_{a/2}$ (V vs. Ag/AgCl)vs. ln ν for third anodic peak (e) Plot of $E_{a/2}$ (V vs. Ag/AgCl)vs. ln ν for fourth anodic peak for complex **3**.

(a) (b)

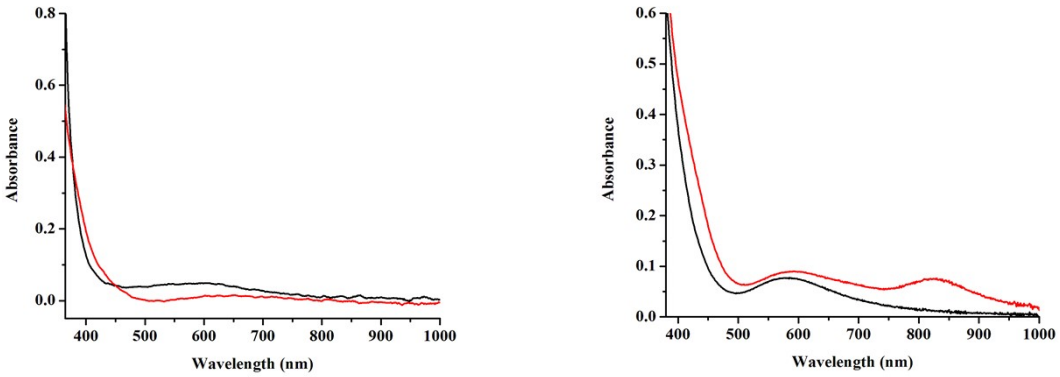

(c)

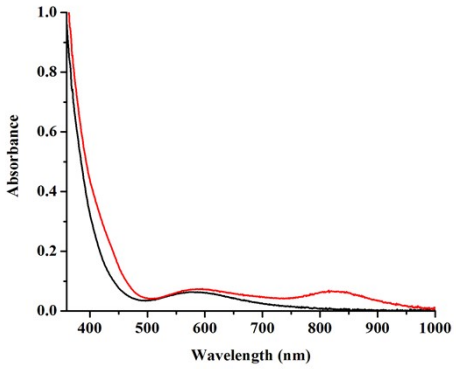

Figure S26. (a) UV-visible spectra of complex **1** after electrolysis at +0.76 V in neutral phosphate buffer at room temperature. **(b)** UV-visible spectra of complex **2** after electrolysis at +0.64V in neutral phosphate buffer at room temperature.**(c)** UV-visible spectra of complex **3** after electrolysis at +0.60 V in neutral phosphate buffer at room temperature.

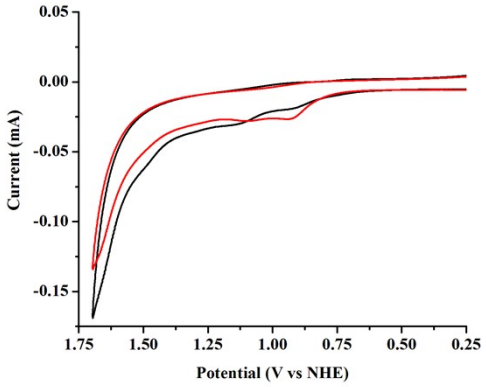

Figure S27. Cyclic voltammogram of complex **1** (black) and analogous Zn^{2+}-complex (red) in neutral phosphate buffer at 100 mV s^{-1} scan rate

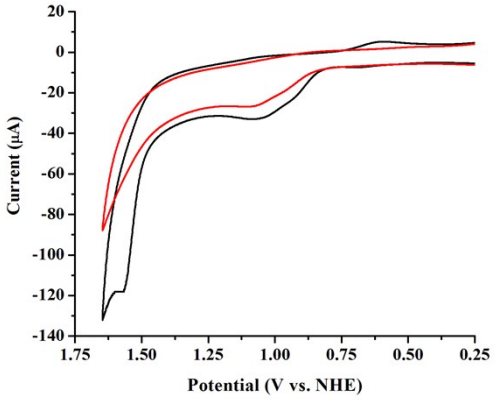

Figure S28. Cyclic voltammogram of complex **2** (black) and analogous Zn^{2+}-complex (red) in neutral phosphate buffer at 100 mV s^{-1} scan rate

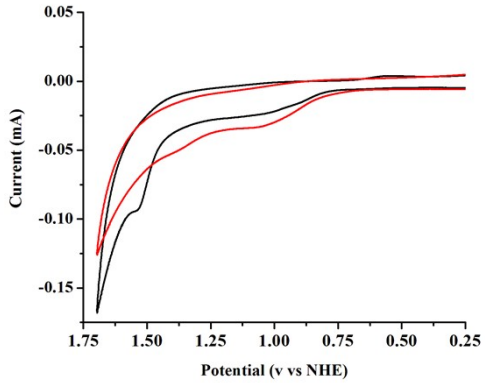

Figure S29. Cyclic voltammogram of complex**3** (black) and analogous Zn^{2+}-complex (red) in neutral phosphate buffer at 100 mV s^{-1} scan rate.

(a)

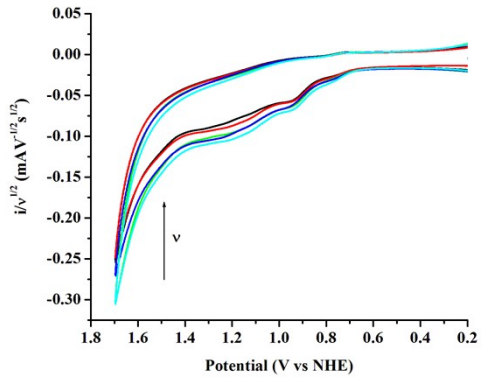

(b)

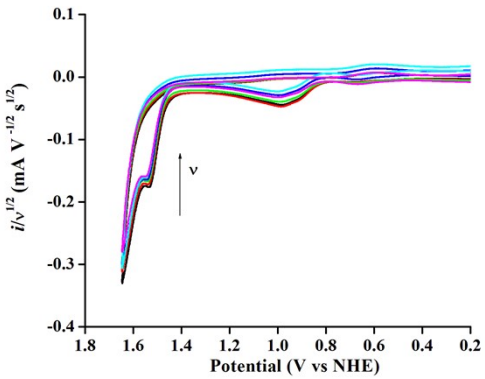

(c)

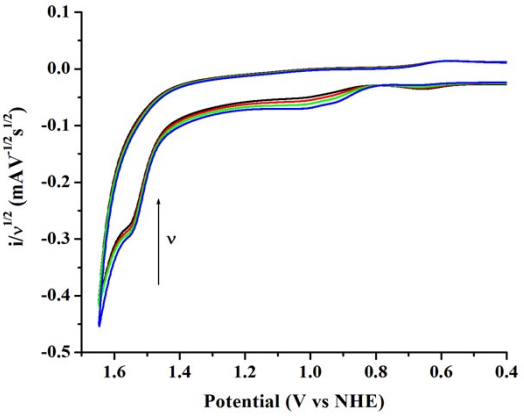

Figure S30. Scan rate normalised CVof (a) complex **1**,(b) complex **2**and (**c**)complex **3**in 0.1 M neutral phosphate buffer.

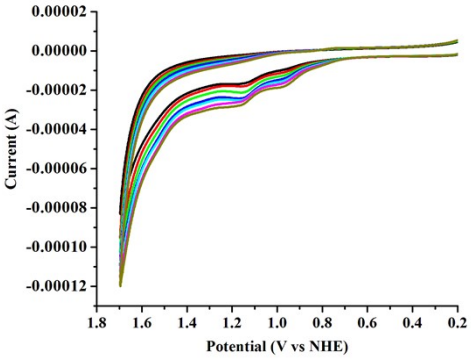

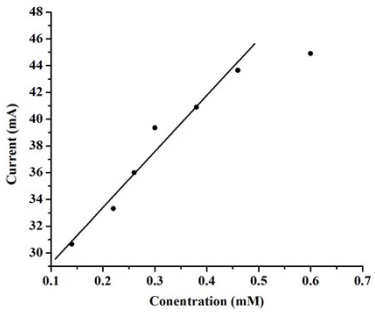

Figure S31. (Left) Background corrected CV of complex**1** at 0.14(black), 0.22 (red), 0.26 (green), 0.30 (blue), 0.38 (cyan), 0.46 (magenta), 0.60mM(olive), concentration in 0.1 M neutral phosphate buffer. Scan rate: 100mV/s.**(Right)** Catalytic current at 1.51V as a function of the catalyst concentration from 0.14 to 0.60mM measured in 0.1 M neutral phosphate buffer.

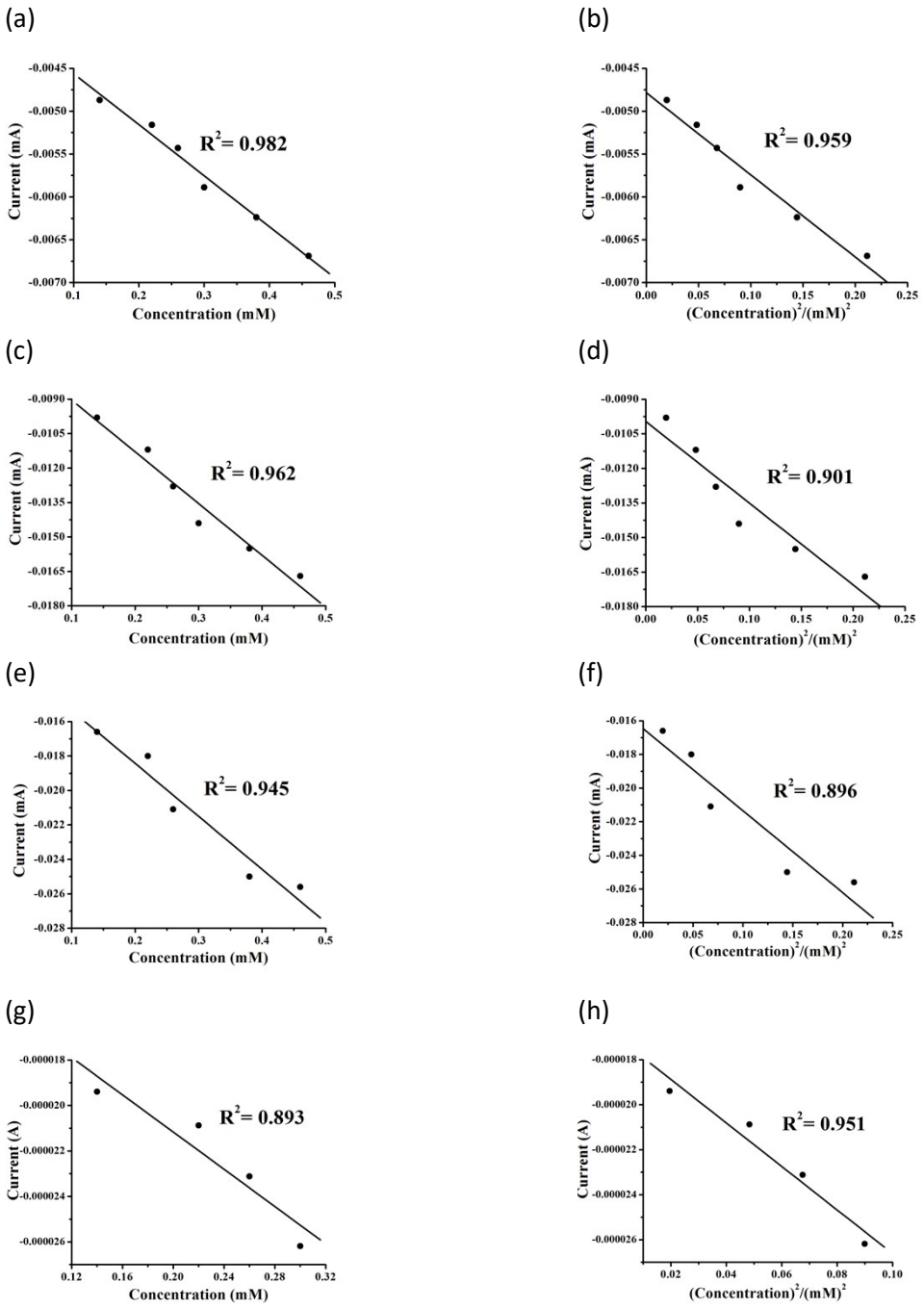

Figure. S32 Plot of current vs. concentration at +0.76V **(a)**, +0.89V **(c)**, +0.97V **(e)** and +1.08V **(g)**.Plot of current vs. square of concentrationat +0.76V **(b)**, +0.89V **(d)**, +0.97V **(f)** and +1.08V **(h)** for complex **1**.

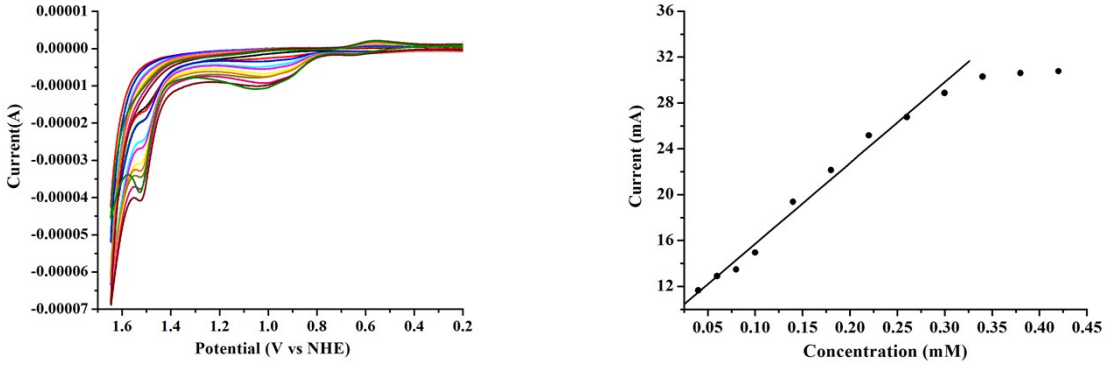

Figure S33. (Left) Background correctedCV of complex**3** at 0.04 (Black) 0.06 (red), 0.08(green), 0.10 (dark blue), 0.14 (light blue), 0.18 (magenta), 0.22 (yellow), 0.26 (dark yellow), 0.30 (orange), 0.34 (pink). 0.38 (wine), 0.42 (olive) mM concentration in 0.1 M neutral phosphate buffer. Scan rate: 100mV/s. **(Right)** Plot of catalytic current at 1.52 V against the concentration of the catalyst for complex **3**

(a) (b)

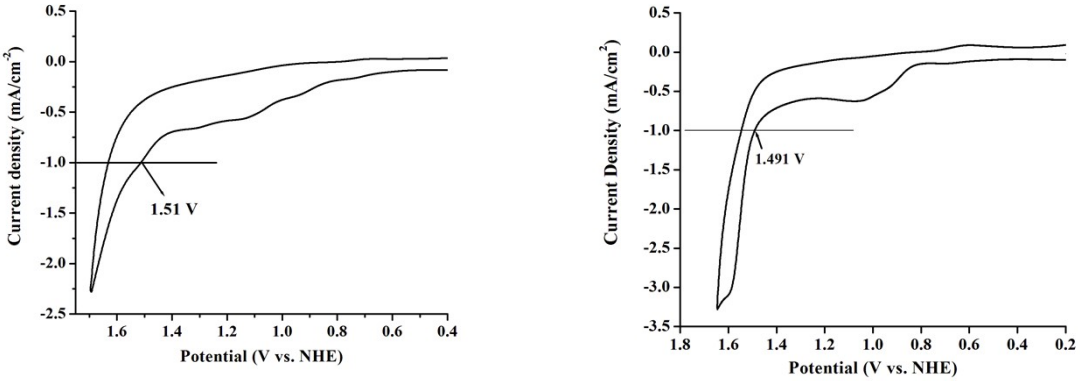

(c)

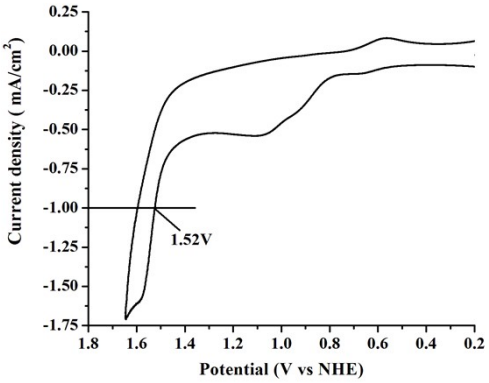

Figure S34. Background correctedCV of complex **1** (a), complex (b) and complex **3** (c) recorded at 1mM concentration in 0.1 M neutral phosphate buffer at 100mV/sec scan rate. The current density of 1mA/cm^{2}was obtained at 1.51V, 1.49V and 1.52 V for complex **1**, **2** and **3**respectively.

(a)

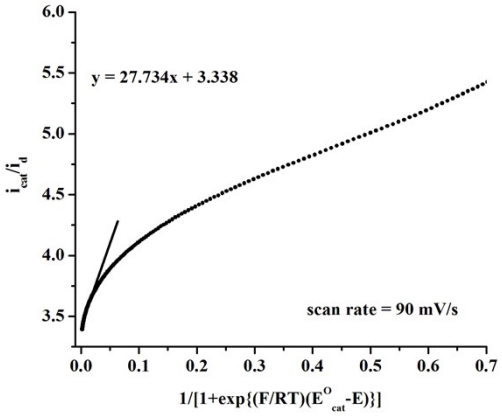

(b)

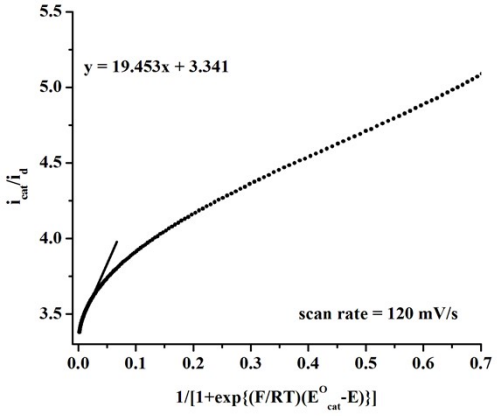

(c)

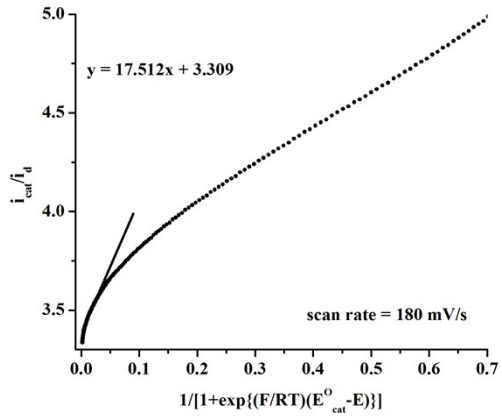

(d)

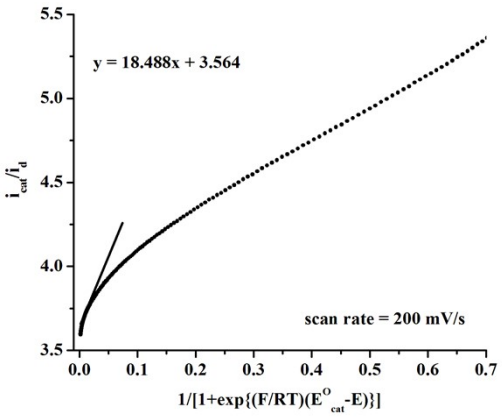

(e)

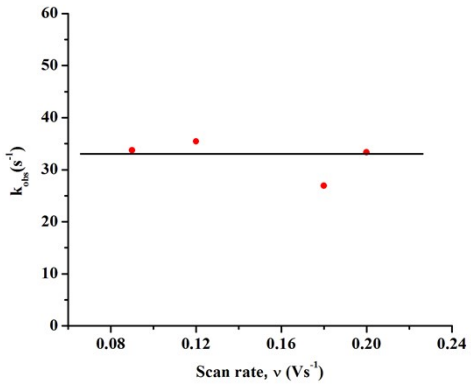

FigureS35 (a) to (d) FOWA for complex **1**. (e) Plot of the different k_{obs} values extracted from the foot-of-the-wave analysis at scan rate 90-200 mVs^{-1}. The black line represents the average k_{obs} value (~32 s^{-1}).

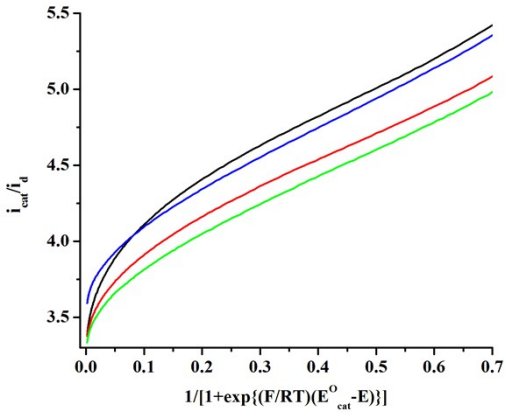

Figure S36. Foot-of-the-wave analysis plotting i_{cat}/i_d vs. $1/[1+\exp\{(F/RT)(E^{o}_{cat}-E)\}]$ at 90 (black), 120 (red), 180 (green) and 200 (dark blue) mVs^{-1} scan rates for complex **1**.

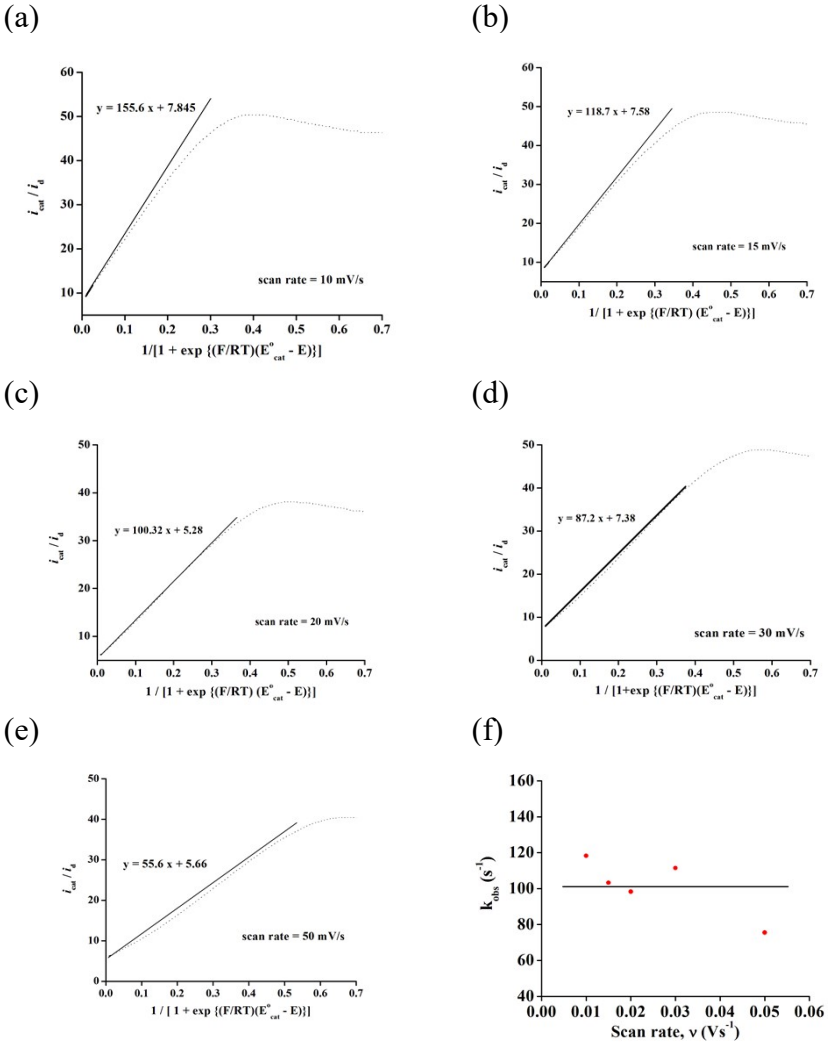

Figure S37. (a) to (e) FOWA. (f) Plot of the different kobs values extracted from the foot-of-the-wave analysis at scan rate 10-50 mVs^{-1} for complex **2**. In figure (f) the black line represents the average k_{obs} value (~100 s^{-1}).

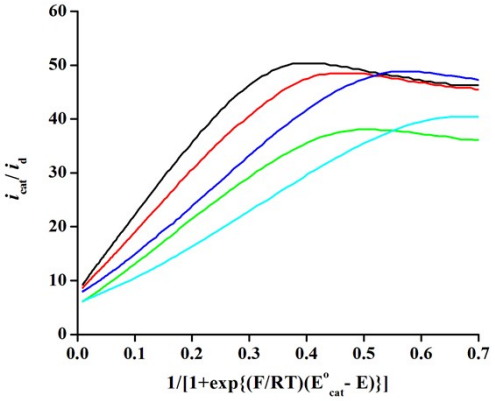

Figure S38 Foot-of-the-wave analysis plotting i_{cat}/i_d vs. 1/[1+exp{(F/RT)(E^o_{cat}-E)}] at 10 (black), 15 (red), 20 (green), 30 (dark blue) and 50 (cyan) mVs^{-1} scan rates for complex **2**

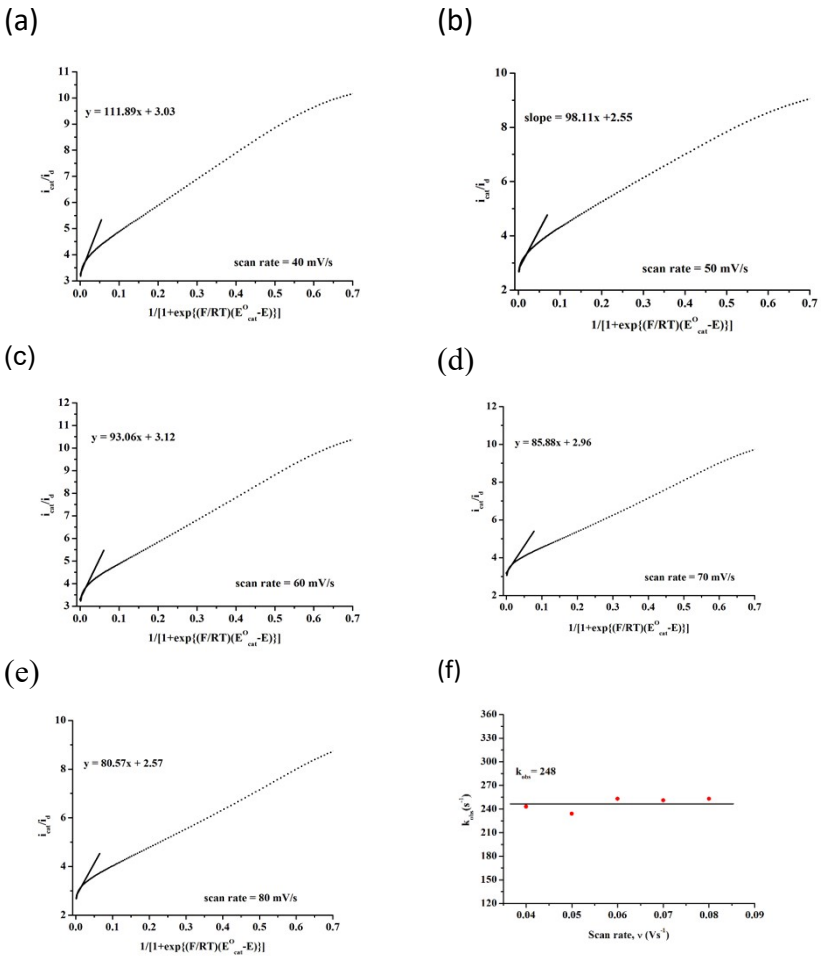

Figure S39. (a) to (e) FOWA for complex **2.** (f) Plot of the different k_{obs} values extracted from the foot-of-the-wave analysis at scan rate 40-80 mVs^{-1} for complex **3**. The black line represents the average k_{obs} value (~248 s^{-1}).

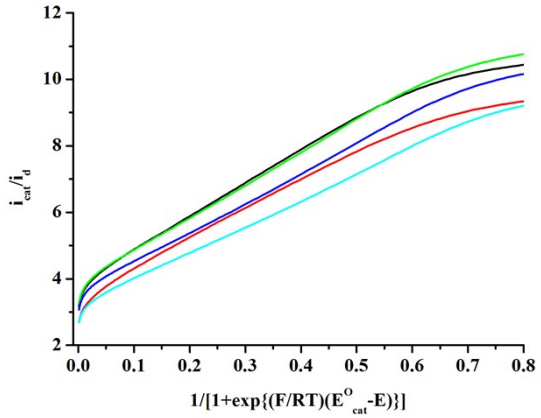

Figure S40. Foot-of-the-wave analysis plotting i_{cat}/i_d vs. $1/[1+\exp\{(F/RT)(E^{o}_{cat}-E)\}]$ at 40 (black), 50 (red), 60 (green),70 (dark blue) and 80 (cyan) mVs^{-1} scan rates for complex **3**.

(a) (b)

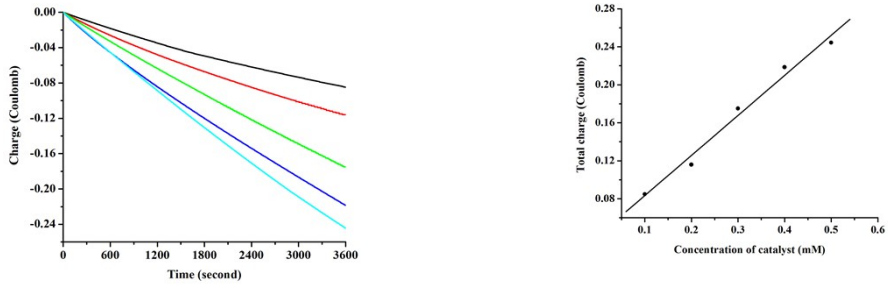

Figure S41. (a) Plot of charge vs. time recorded during bulk electrolysis of complex **1** at 0.1mM (black), 0.2mM (red), 0.3mM (green), 0.4mM (dark blue) and 0.5mM (light blue) concentration at 1.51 V vs. NHE in 0.1 M neutral phosphate buffer. (**b)** Plot of total charge vs. concentration of complex **1** after 1h of electrolysis

(a) (b)

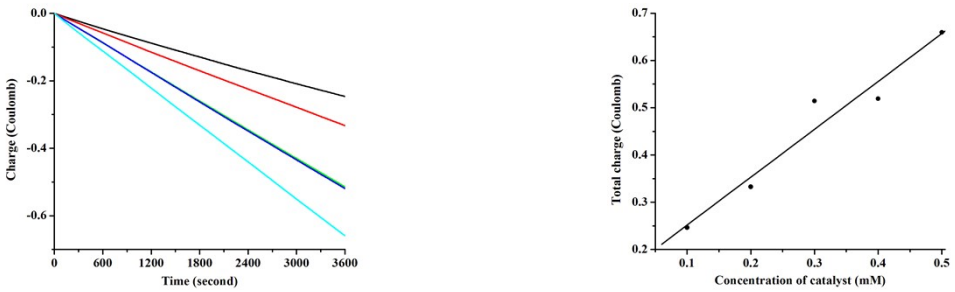

Figure.S42 (a) Plot of charge vs. time recorded during bulk electrolysis of complex **2** at 0.1mM (black), 0.2mM (red), 0.3mM (green), 0.4mM (dark blue) and 0.5mM (light blue) concentration at 1.49 V vs. NHE in 0.1 M neutral phosphate buffer. (**b)** Plot of total charge vs. concentration of complex **2** after 1h of electrolysis.

(a) (b)

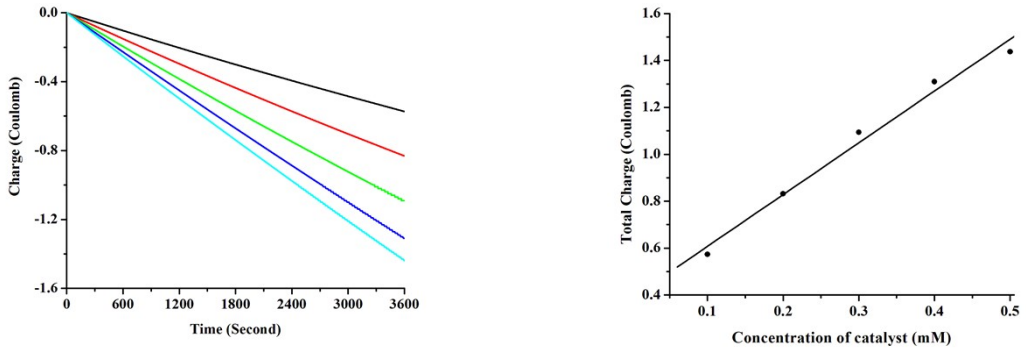

Figure.S43 (a) Plot of charge vs. time recorded during bulk electrolysis of complex **3** at 0.1mM (black), 0.2mM (red), 0.3mM (green), 0.4mM (dark blue) and 0.5mM (light blue) concentration at 1.52 V vs. NHE in 0.1 M neutral phosphate buffer. (**b)** Plot of total charge vs. concentration of complex **3** after 1h of electrolysis.

(a) (b)

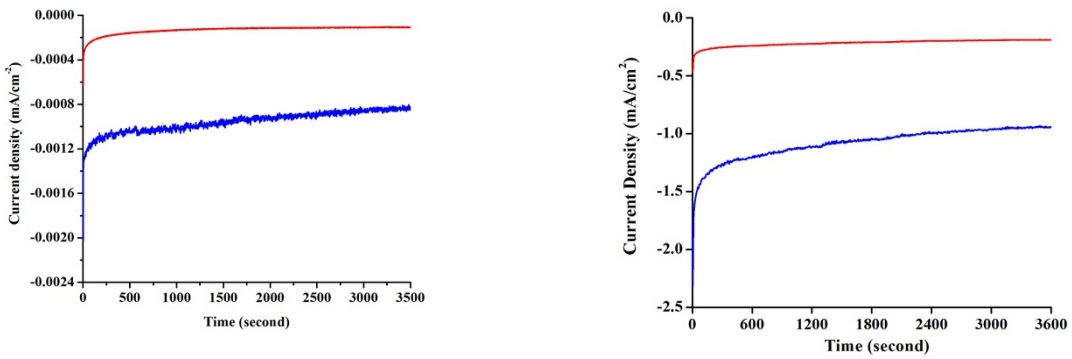

(c)

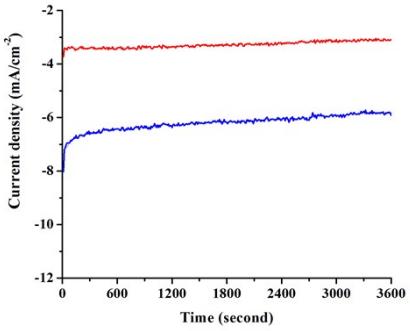

Figure S44. Plot of current density vs. time obtained frombulk electrolysis experiment with (blue line) and without (red line) complex **1**(a), complex **2** (b) and complex **3** (c) in 0.1 M neutral phosphate buffer using ITO working electrode (area 4 cm^2) at 1.51 V, 1.49 V and 1.52 V respectively

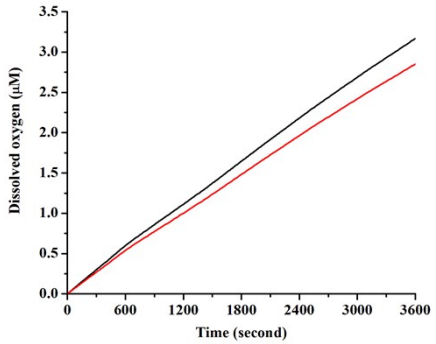

Figure S45. Plot of concentration of Oxygen evolved against time during bulk electrolysis experiment at 1.52 V versus NHE with complex **1** in0.1 M neutral phosphate buffer (red line). The black line indicates the theoretical amount of oxygen as assumed by charge passed with 100% faradaic efficiency.

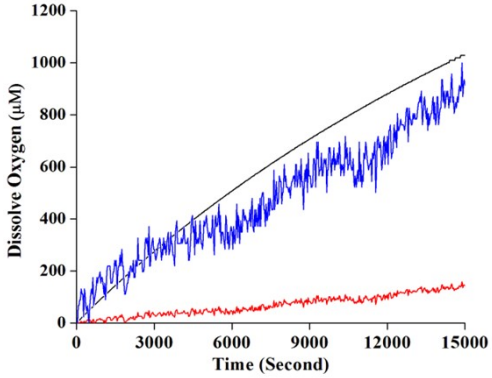

Figure S46. Plot of concentration of Oxygen evolved against time during bulk electrolysis experiment at 1.49 V versus NHE with (blue line) and without (red line) complex **2** in0.1 M neutral phosphate buffer. The black line indicates the theoretical amount of oxygen as assumed by charge passed with 100% faradaic efficiency.

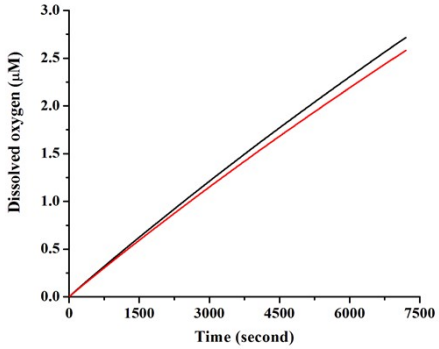

Figure S47. Plot of concentration of Oxygen evolved against time during bulk electrolysis experiment at 1.52 V versus NHE with complex **3** in0.1 M neutral phosphate buffer (red line). The black line indicates the theoretical amount of oxygen as assumed by charge passed with 100% faradaic efficiency.

(a)

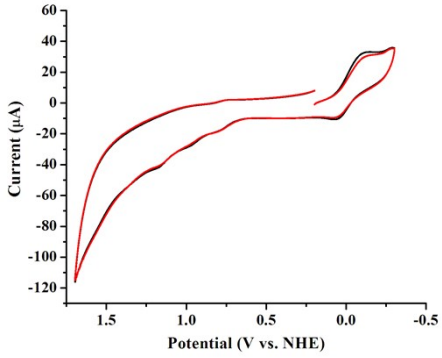

(b)

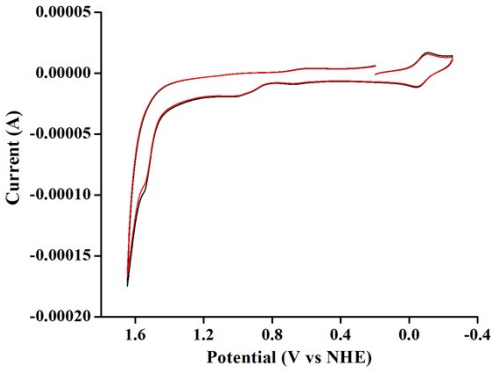

(c)

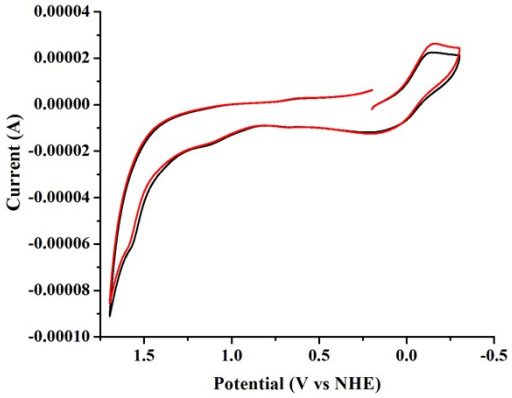

Figure S48. (a)Cyclic voltammogram of complex **1**before (black line) and after (red line) electrolysis at 1.51 V vs. NHE in 0.1 M neutral phosphate buffer. (b) Cyclic voltammogram of complex **2** before (black line) and after (red line) electrolysis at 1.49 V vs. NHE in 0.1 M neutral phosphate buffer. (c) Cyclic voltammogram of complex **3** before (black line) and after (red line) electrolysis at 1.52 V vs. NHE in 0.1 M neutral phosphate buffer.

(a)

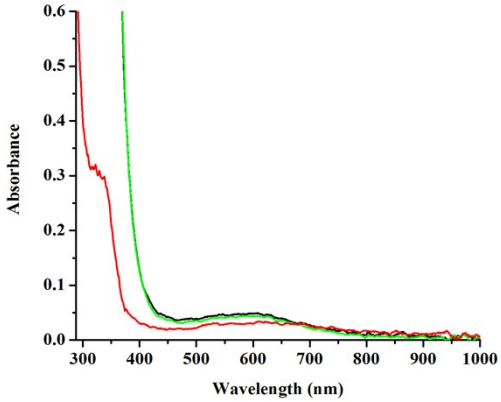

(b)

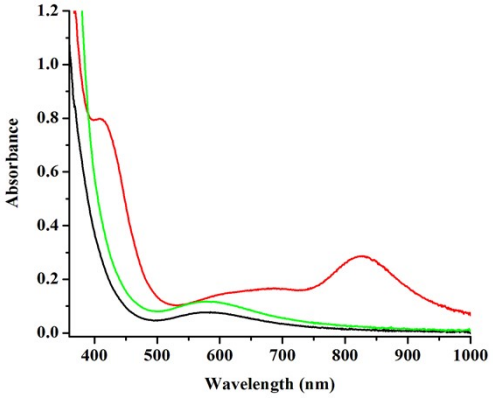

(c)

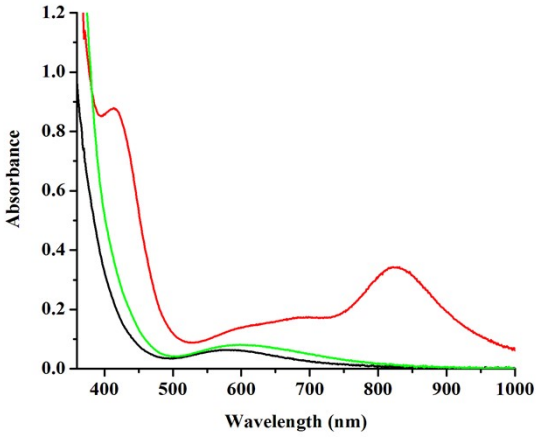

Figure S49. **(a)** UV-visible spectra of complex **1** before electrolysis (black), just after completion of electrolysis (red) and after 1h of completion of electrolysis (green) at 1.51 V vs. NHE in 0.1 M neutral phosphate buffer. **(b)** UV-visible spectra of complex **2** before electrolysis (black), just after completion of electrolysis (red) and after 1h of completion of electrolysis (green) at 1.49 V vs. NHE in 0.1 M neutral phosphate buffer. **(c)** UV-visible spectra of complex **3** before electrolysis (black), just after completion of electrolysis (red) and after 1h of completion of electrolysis (green) at 1.52 V vs. NHE in 0.1 M neutral phosphate buffer.

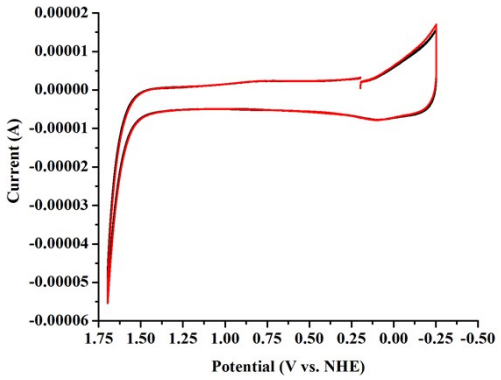

Figure S50. Cyclic voltammogram recorded in 0.1 M neutral phosphate buffer with fresh (black line) and used (red line) ITO working electrode (area 4 cm^2) for complex **1**

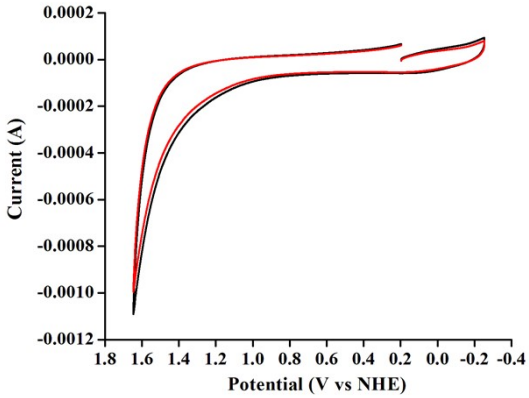

Figure S51. Cyclic voltammogram recorded in 0.1 M neutral phosphate buffer with fresh (black line) and used (red line) ITO working electrode (area 4 cm^2) for complex **2**

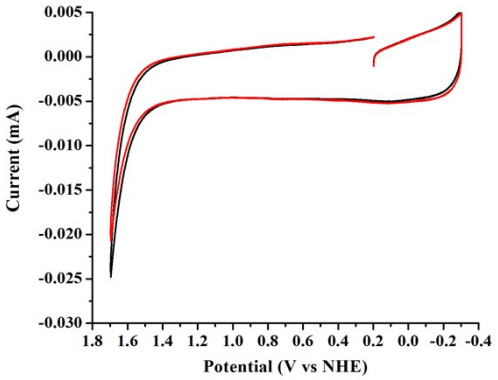

Figure S52. Cyclic voltammogram recorded in 0.1 M neutral phosphate buffer with fresh (black line) and used (red line) ITO working electrode (area 4 cm^2) for complex **3**.

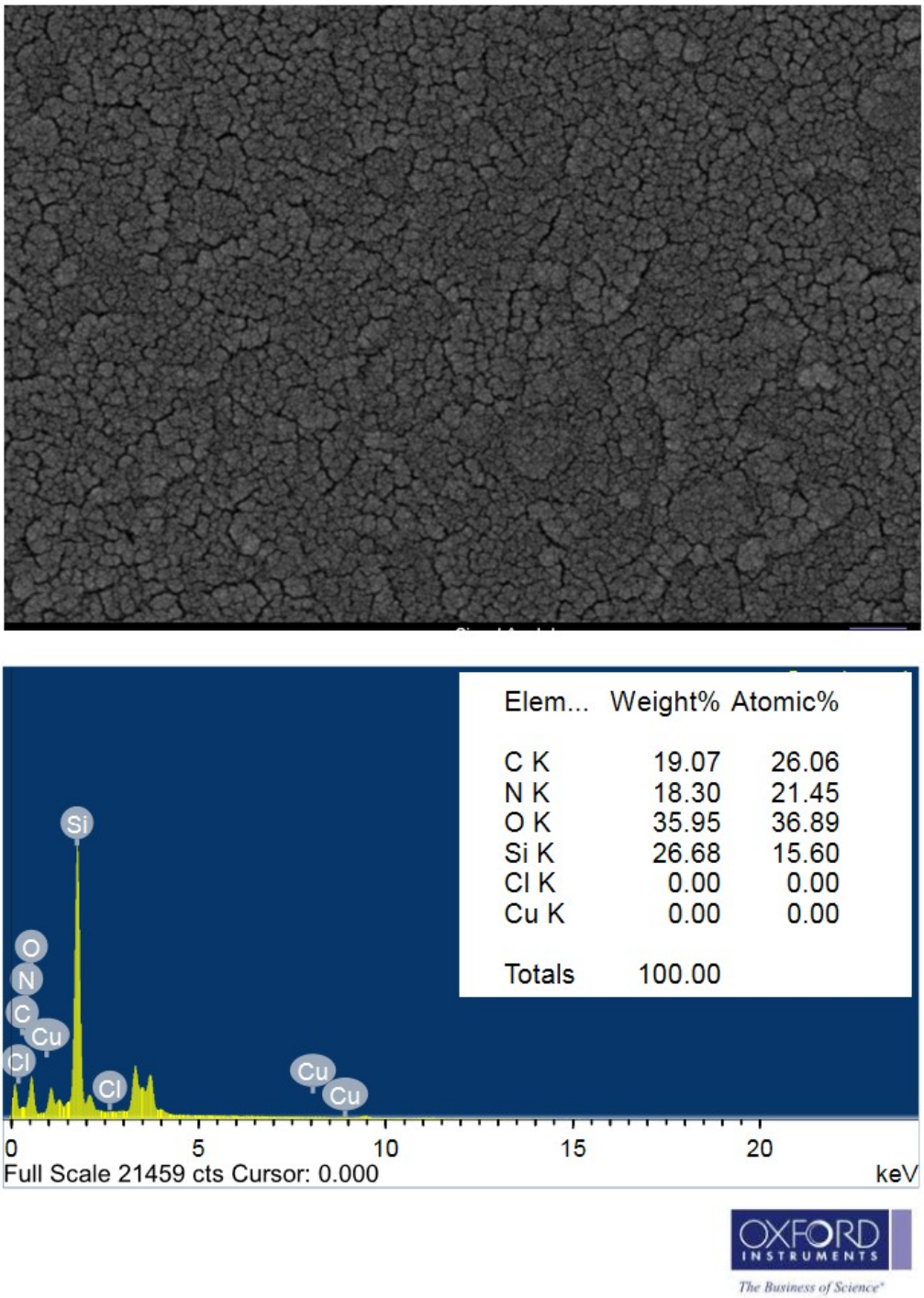

Figure S53.FE-SEM and EDX plot of fresh ITO sample before electrolysis experiment of complex**1** in neutral phosphate buffer.

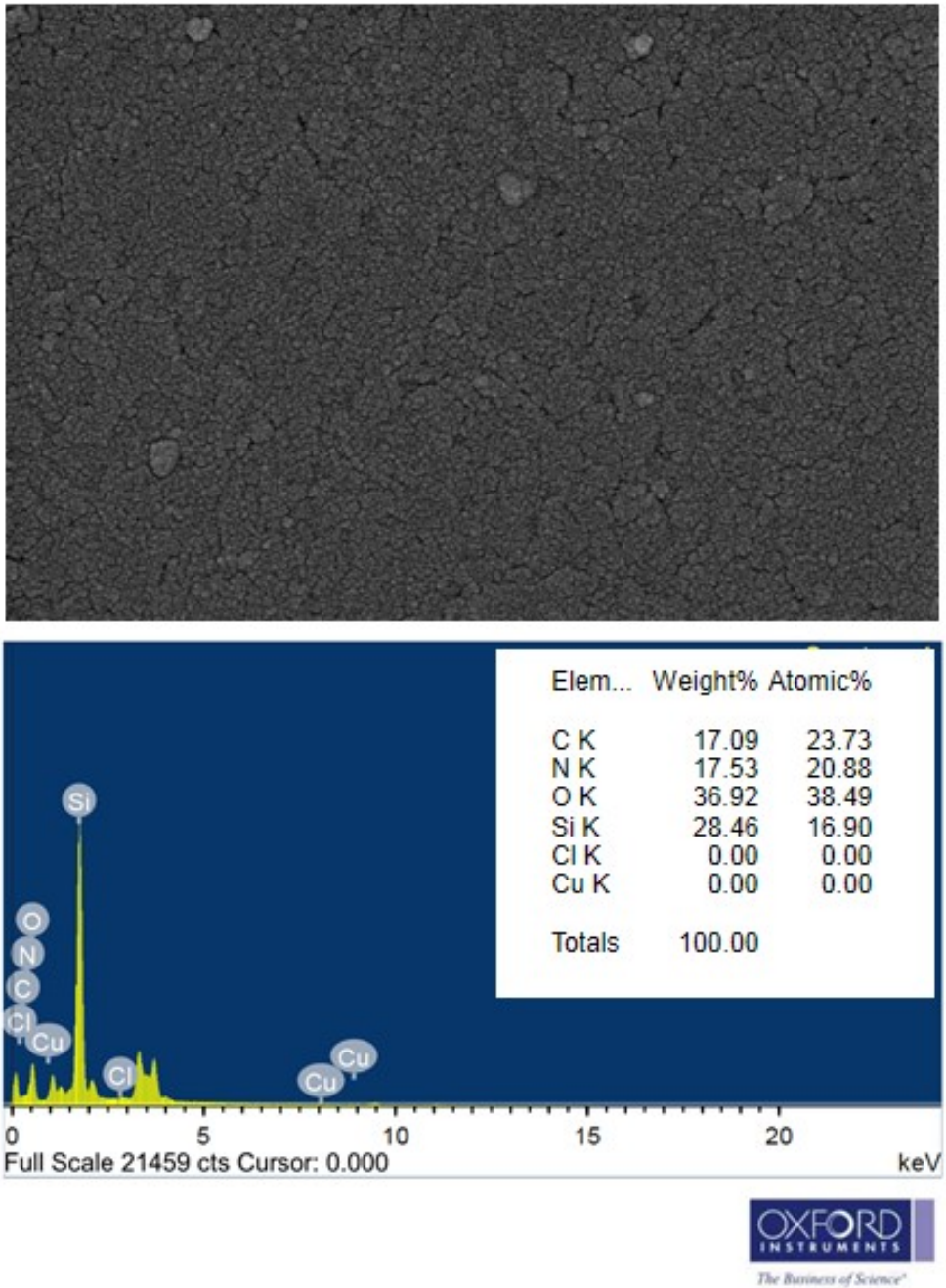

FigureS54 FE-SEM and EDX plot of used ITO sample after electrolysis experiment of complex **1**in neutral phosphate buffer.

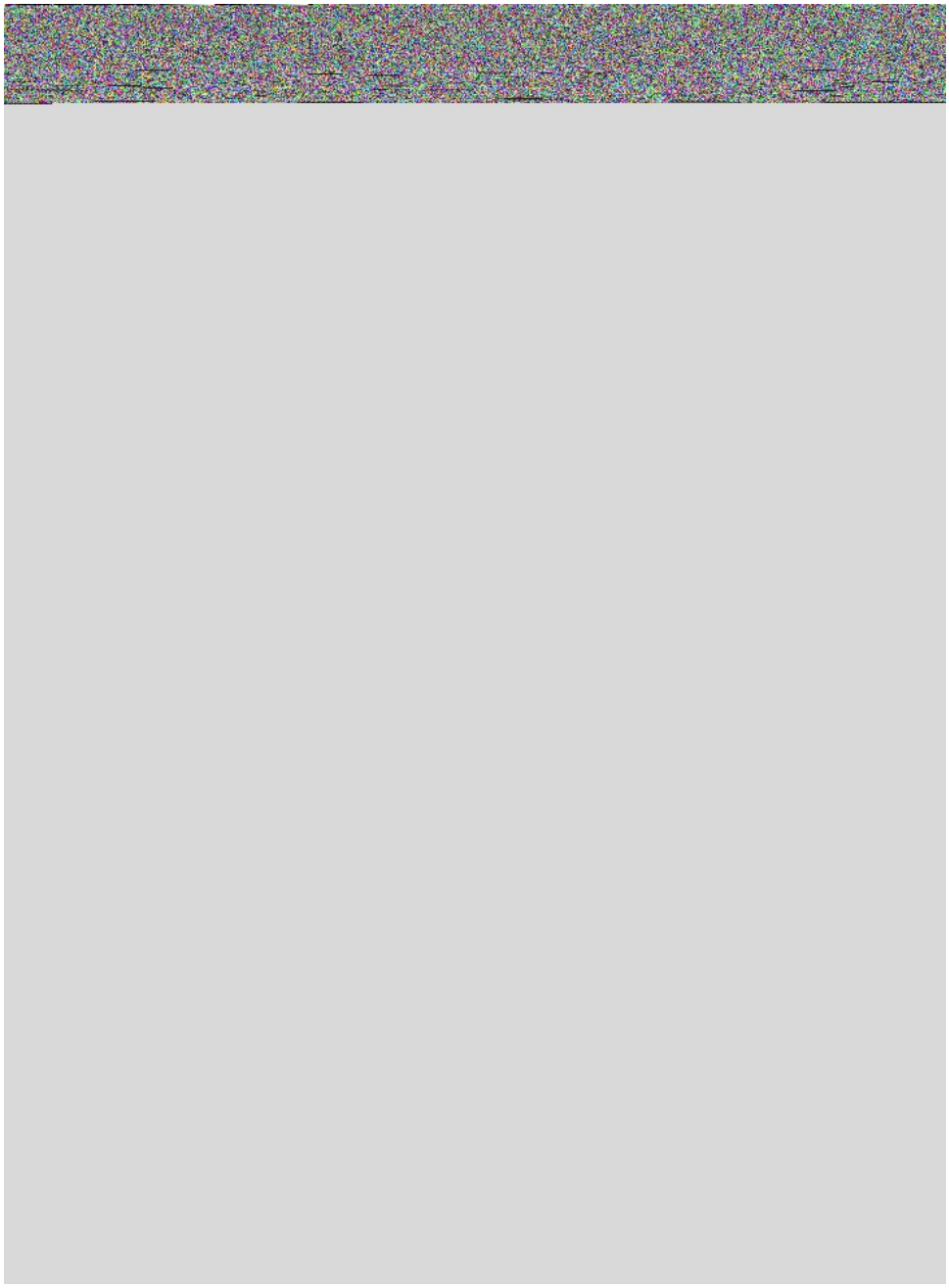

Figure S55FE-SEM and EDX plot of fresh ITO sample before electrolysis experiment of complex **2** in neutral phosphate buffer.

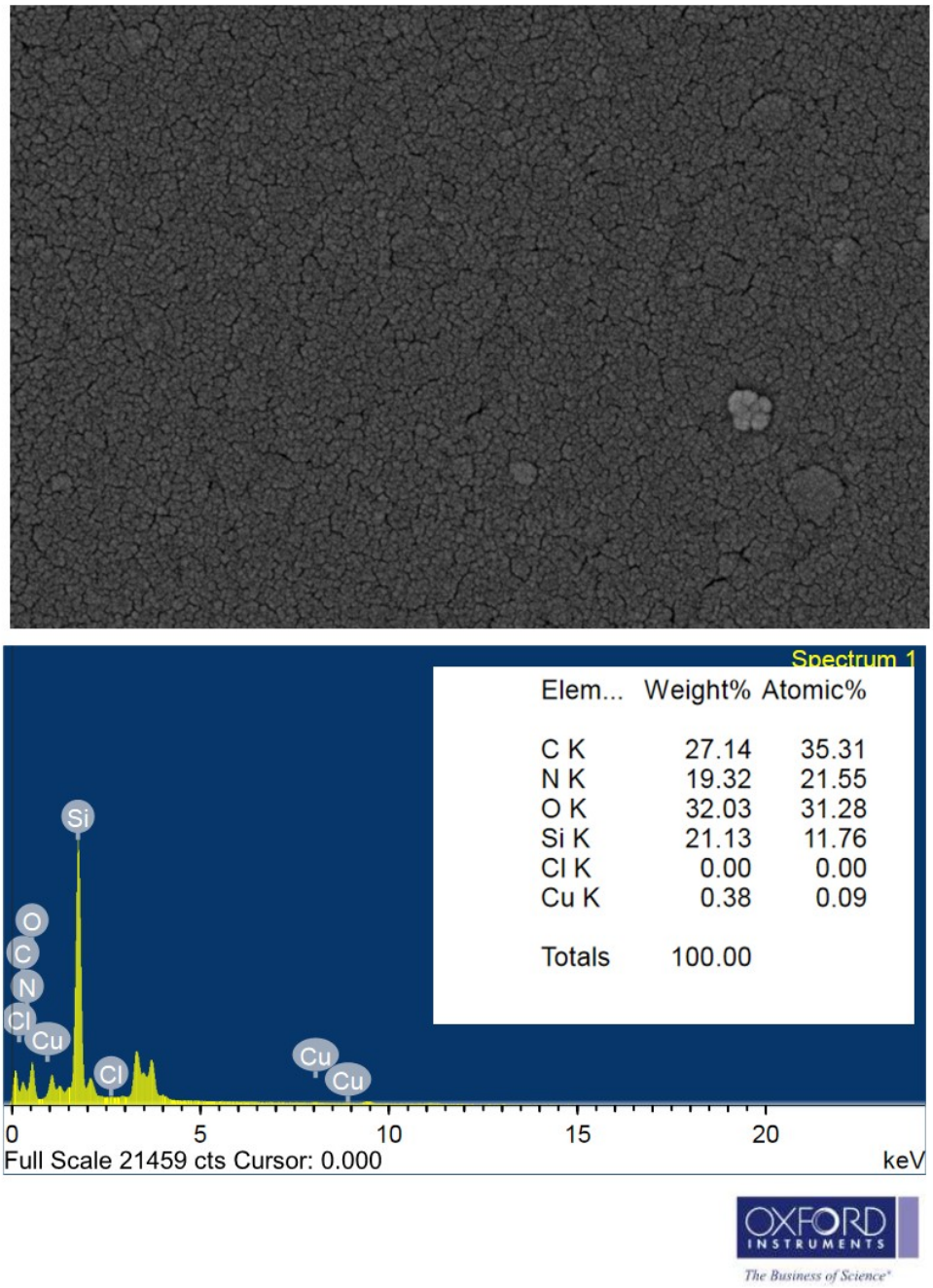

Figure S56. FE-SEM and EDX plot of used ITO sample after electrolysis experiment of complex **2** in neutral phosphate buffer.

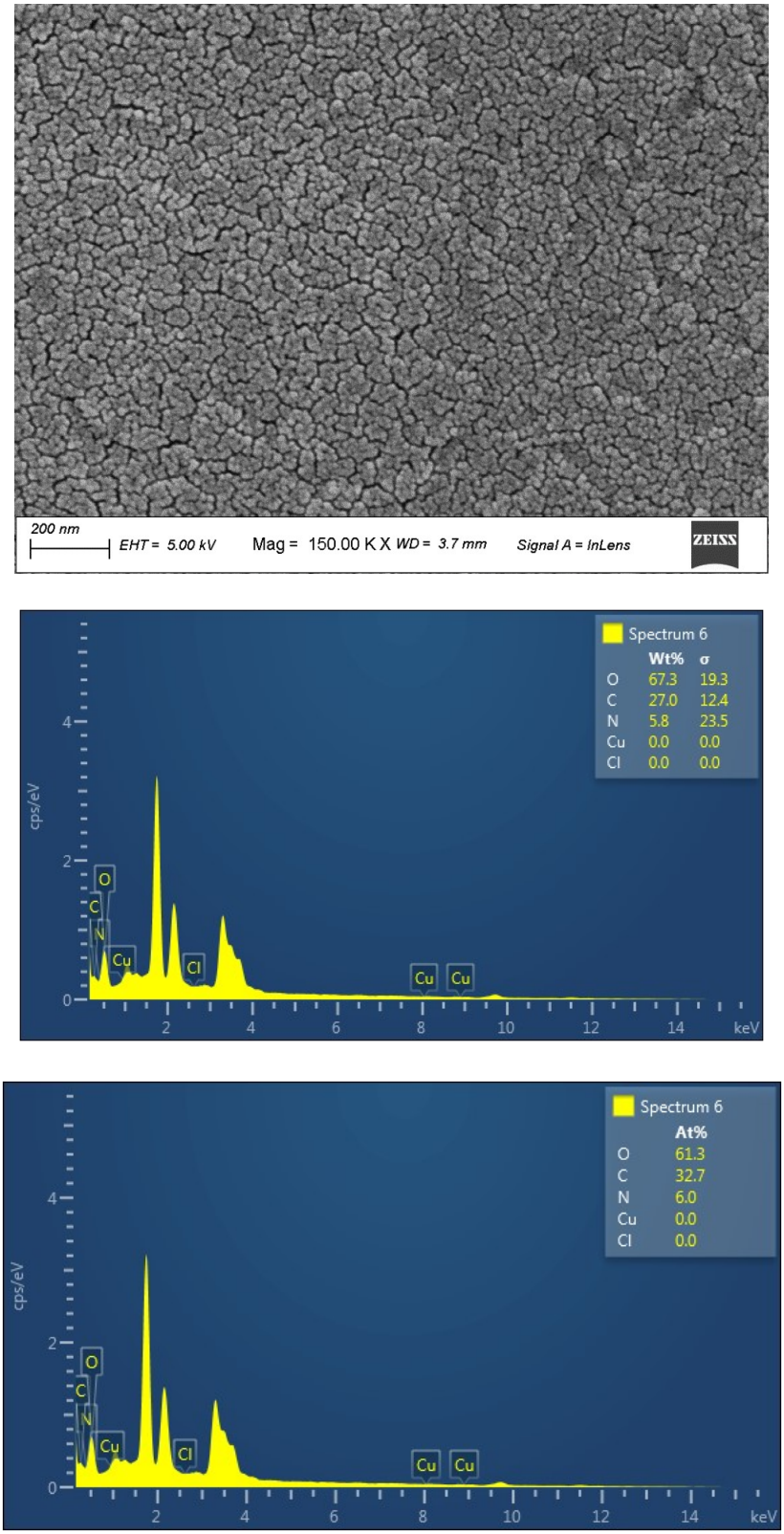

Figure S57.FE-SEM and EDX plot of fresh ITO sample before electrolysis experiment of complex **3** in neutral phosphate buffer.

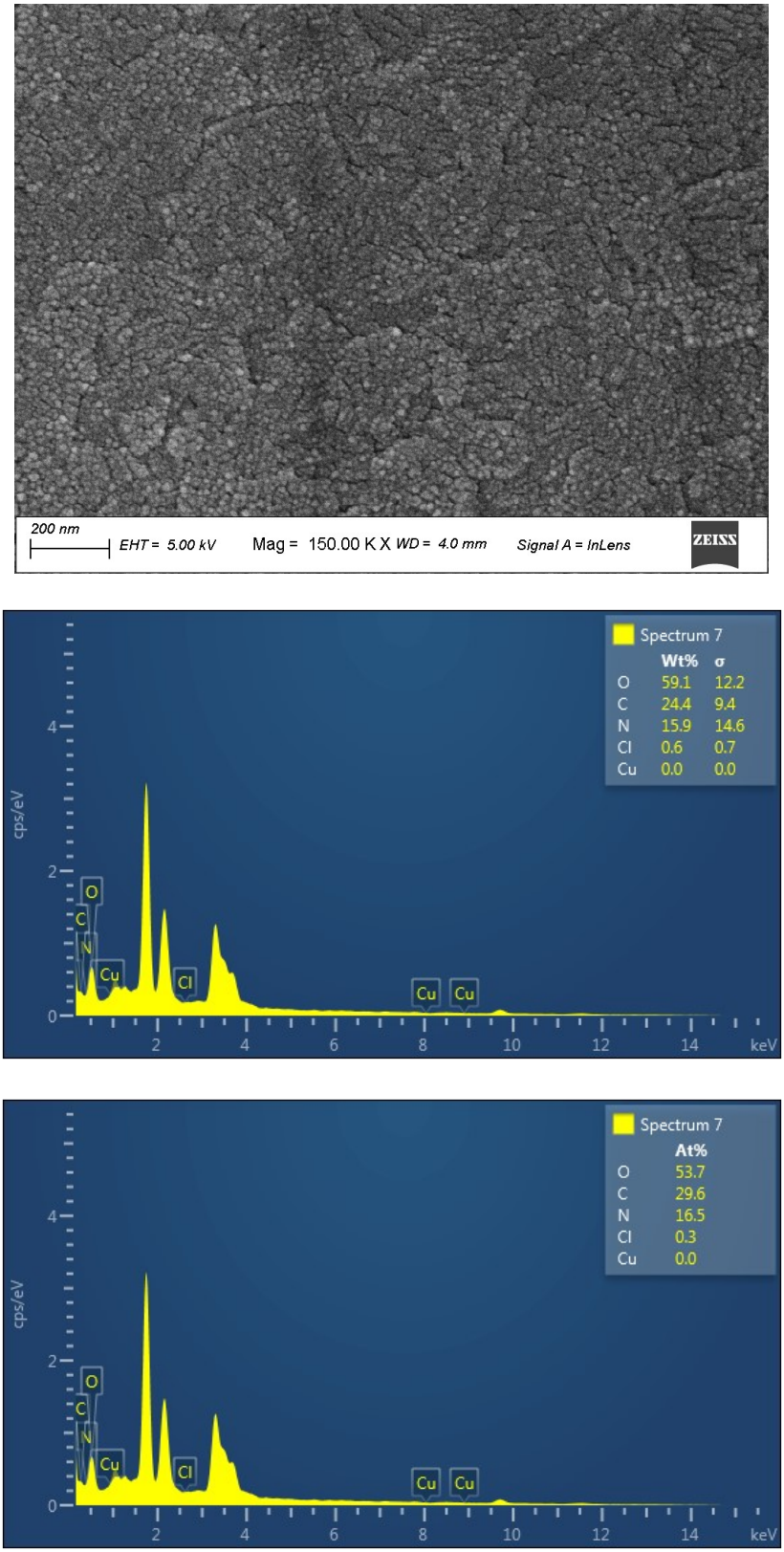

Figure S58.FE-SEM and EDX plot of used ITO sample after electrolysis experiment of complex **3** in neutral phosphate buffer.

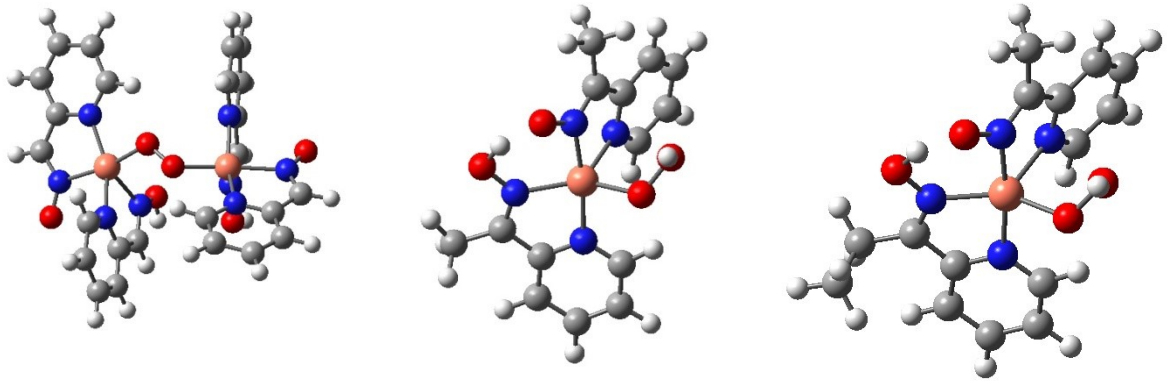

(a) (b) (c)

Figure S59. DFT optimised structure of metal peroxo intermediates generated from (a) Complex **1**, (b) Complex **2** and (c) Complex **3**.

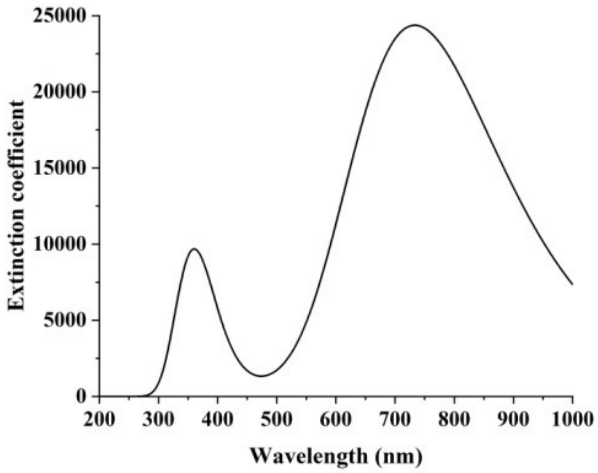

Figure S60. UV-visible spectrum obtained from TDDFT calculations carried out on the DFT optimized structures of metal peroxo intermediates generated from complex **1** during its catalytic cycle. Peak at 358 nm is assigned for the electronic transition from HOMO-20 to LUMO.

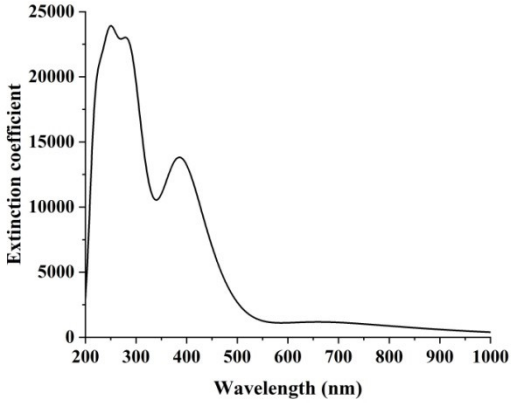

Figure S61. UV-visible spectrum obtained from TDDFT calculations carried out on the DFT optimized structures of metal peroxo intermediates generated from complex 2 during its catalytic cycle. Peak at 385 nm is assigned for the electronic transition from HOMO-1 to LUMO.

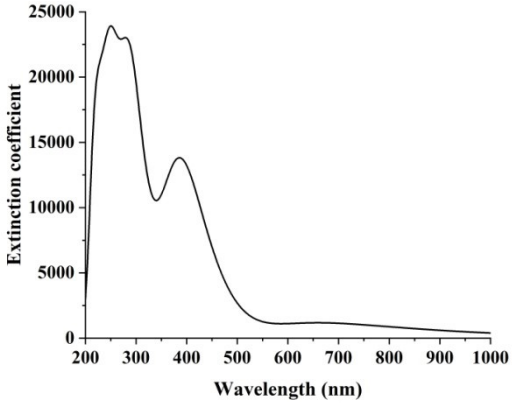

Figure S62. UV-visible spectrum obtained from TDDFT calculations carried out on the DFT optimized structures of metal peroxo intermediates generated from complex 3 during its catalytic cycle. Peak at 387 nm is assigned for the electronic transition from HOMO-1 to LUMO.

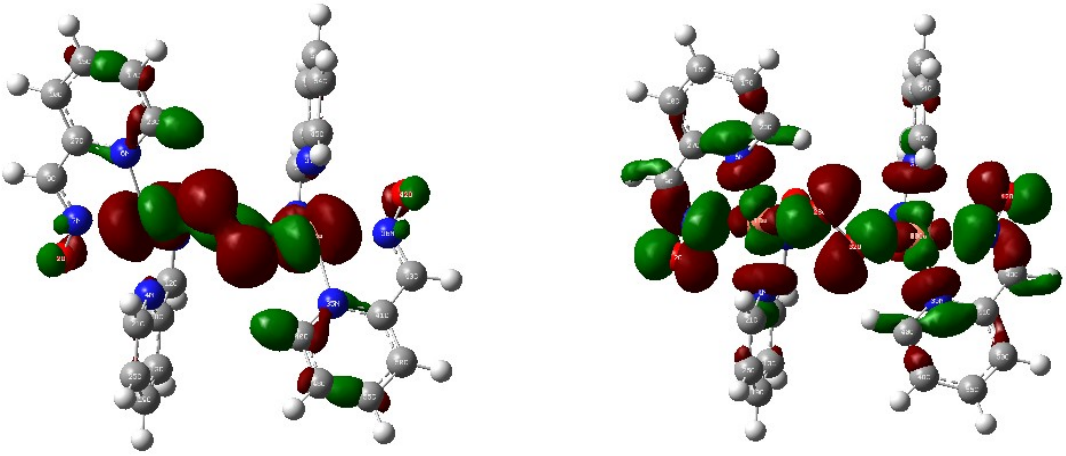

(a) (b)

Figure S63. (a) Boundary surface diagram of HOMO-20 orbital calculated from the DFT optimized structure of the metal peroxo intermediated generated from complex **1**showing interaction between π* orbital of the peroxide ion with a d orbital of the metal center. **(b)**Boundary surface diagram of LUMO calculated from the DFT optimized structure of the metal peroxo intermediated generated from complex **1.**

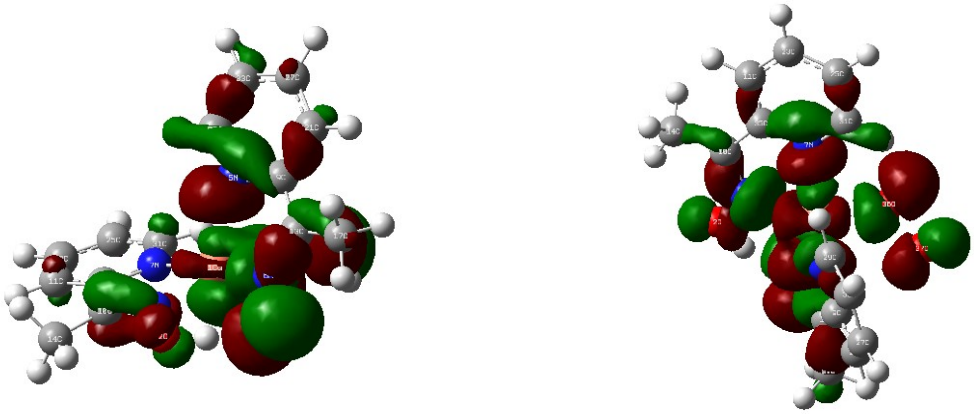

(a) **(b)**

Figure S64. (a) Boundary surface diagram of HOMO-1 orbital calculated from the DFT optimized structure of the metal peroxo intermediated generated from complex **2** showing interaction between π* orbital of the peroxide ion with a d orbital of the metal center. **(b)** Boundary surface diagram of LUMO calculated from the DFT optimized structure of the metal peroxo intermediated generated from complex 2**.**

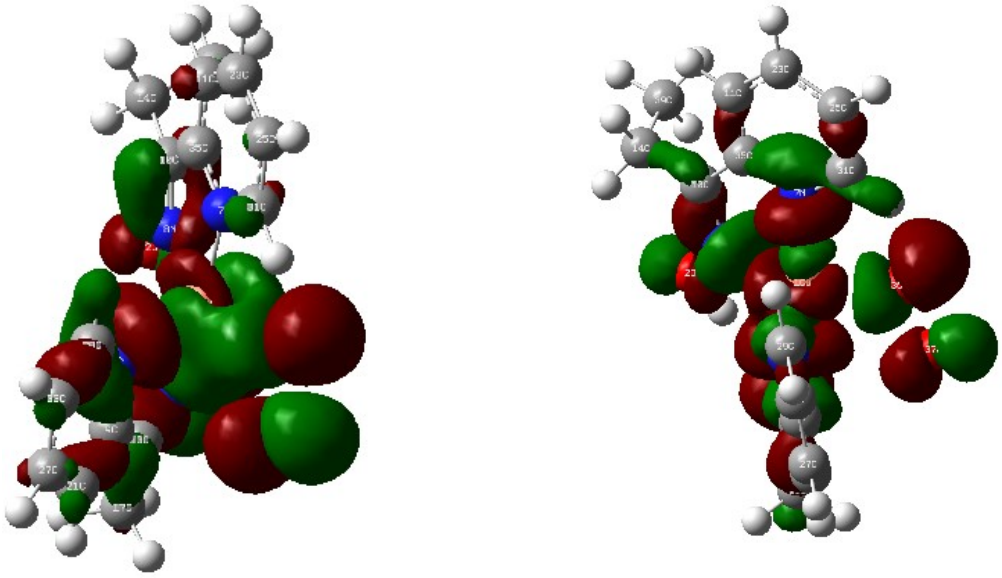

(a) (b)

Figure S65. (a) Boundary surface diagram of HOMO-1 orbital calculated from the DFT optimized structure of the metal peroxo intermediated generated from complex **3** showing interaction between π* orbital of the peroxide ion with a d orbital of the metal center. **(b)** Boundary surface diagram of LUMO calculated from the DFT optimized structure of the metal peroxo intermediated generated from complex **3.**

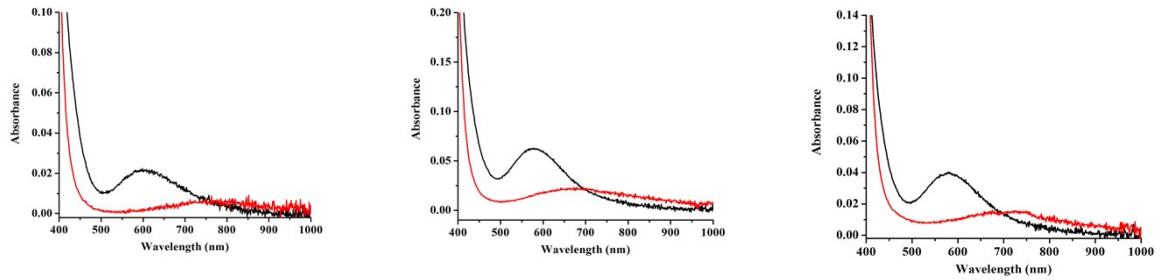

(a) (b) (c)

Figure S66 (a) UV-visible spectra of complex **1** before (black line) and after (red line) reaction with Cerric ammonium nitrate in aqueous medium. **(b)** UV-visible spectra of complex **2** before (black line) and after (red line) reaction with Cerric ammonium nitrate in aquous medium. **(c)** UV-visible spectra of complex **3** before (black line) and after (red line) reaction with Cerric ammonium nitrate in aqueous medium.

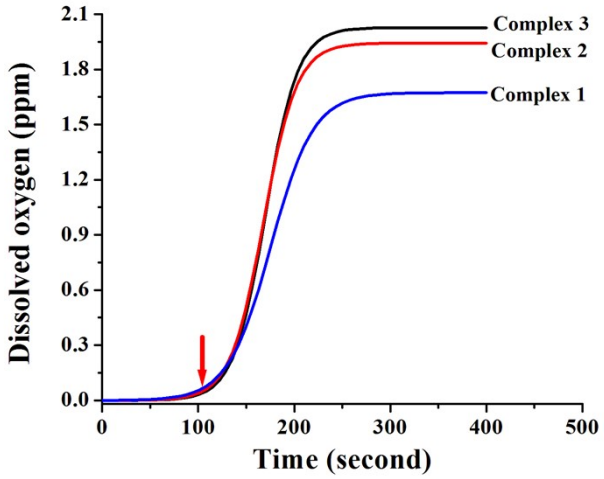

Figure S67. Plot of concentration of Oxygen evolved against time after addition of 10 ml degassed 1 mM aqueous solution of the metal complexes to 40 mL degassed 100 mM aqueous solution of Cerium ammonium nitrate (CAN) in a gas-tight cell equipped with magnetic stirring bar and calibrated Ocean Optics FOXY probe. The arrow corresponds to the point of addition of the complex solution.

Table S1. Total charge passed through working electrode after 1h of electrolysis of complex 1, 2 and 3 at the E_{cat} potential.

Concentration of the catalysts (mM)	**Total Charge of the catalyst after 1h of bulk electrolysis (Coulomb)**		
	Complex 1	**Complex 2**	**Complex 3**
0.1	-0.084	-0.246	-0.573
0.2	-0.116	-0.332	-0.831
0.3	-0.175	-0.514	-1.093
0.4	-0.218	-0.519	-1.309
0.5	-0.244	-0.659	-1.437

Table S2. Crystal data and structure refinement parameters for Complex **1**, **2** and **3**

	Complex 1	**Complex 2**	**Complex 3**
Empirical formula	$CuN_4O_6C_{12}H_{10}Cl$	$CuN_4O_7C_{14}H_{17}Cl$	$CuN_4O_6C_{15}H_{17}Cl$
Formula weight	405.23	452.30	448.32
Wavelength(λ)	0.71073 Å	0.71073 Å	0.71073 Å
Temperature	273(2) K	293(2) K	300(2) K
Crystal system	Trigonal	Monoclinic	Orthorhombic
Space group	$P3_121$	Pc	$P2_1\,2_1\,2_1$

a[Å]	8.5947(7)	6.3587(2)	6.9279(6)
b[Å]	8.5947(7)	15.7475(6)	12.5890(11)
c[Å]	17.7141(14)	9.8349(4)	20.2730(18)
α[°]	90	90	90
β[°]	90	101.219(2)	90
γ[°]	120	90	90
Volume[$Å^3$]	1133.2(2)	965.99(6)	1768.1(3)
Z	3	2	4
Density [Mg/m^3]	1.781	1.555	1.684
Abs. coeff. [mm^{-1}]	1.661	1.312	1.429
Abs. correction	Semi-empirical from equivalents	Semi-empirical from equivalents	Semi-empirical from equivalents
F(000)	612	462	916
Reflections collected / unique	12466 / 1245	9962/2950	16186/3553
R_{int}	0.0388	0.1134	0.0481
Data / restraints / parameters	1245 / 0 / 114	2950 / 79 / 246	3553 / 74 / 246
Min. 2θ/°	2.968	2.476	2.580
Max. 2θ/°	24.723	27.773	26.351
Ranges (h, k, l)	-10<=h<=10, -10<=k<=10, -20<=l<=20	-7<=h<=8, -18<=k<=19, -12<=l<=10	-8<=h<=8, -15<=k<=15, -25<=l<=25
Complete to 2θ (%)	96.8 %	94.1 %	
Refinement method	Full-matrix least-squares on F^2	Full-matrix least-squares on F^2	Full-matrix least-squares on F^2
Goof (F^2)	1.044	1.039	1.067
Final *R* indices [$I>2\sigma(I)$]	R_1 = 0.0203, wR_2 = 0.0456	R_1 = 0.0694, wR_2 = 0.1779	R_1 = 0.0734, wR_2 = 0.1871
R indices (all data)	R_1 = 0.0224, wR_2 = 0.0464	R_1 = 0.0741, wR_2 = 0.1836	R_1 = 0.0816, wR_2 = 0.1990
CCDC No.	2362016	1879870	2285154

[a]$R_1 = \Sigma(||F_0| - |FC||)/\Sigma|F_0|$; [b]$wR_2 = [\Sigma w(|F_0|^2 - |FC|^2)^2/(\Sigma w|F_0|^2)^2]^{1/2}$.

Table S3. Coordinate file of the DFT optimized structure of metal oxo intermediate generated in the catalytic cycle of complex **3**.

Cu	0.00000000	0.00000000	0.00000000
O	0.00000000	0.00000000	2.96235735
O	3.21606334	0.00000000	0.38361866
N	-0.26574464	1.87922005	0.51420063
N	2.21883428	0.80231757	0.50907660
N	0.23639586	-1.88227775	-0.43622703
N	0.11036840	-0.79903117	1.94668960

C	0.79236959	2.64029939	0.94792341
C	0.29697846	-2.10743195	1.95989454
C	0.57547952	-4.10717791	0.41917519
H	0.68680257	-4.78169979	1.26037412
C	2.13781391	2.02769150	0.96981726
C	0.42327925	-2.88599010	3.24445724
H	0.31516576	-2.22787665	4.10931968
H	-0.34877311	-3.66334493	3.30457170
C	3.36303439	2.73726694	1.52265752
H	3.35967466	3.78127629	1.18814813
H	4.25557173	2.27019929	1.09113076
C	0.57662820	3.97794547	1.33398230
H	1.40425676	4.58512918	1.67941339
C	0.63102185	-4.59264270	-0.90143555
H	0.78654817	-5.65169625	-1.08375616
C	0.48542303	-3.70154819	-1.97972378
H	0.52410543	-4.04476325	-3.00731916
C	-0.71472186	4.52586543	1.25750756
H	-0.88616226	5.55655177	1.55285223
C	-1.51010825	2.40948554	0.41406592
H	-2.28662825	1.76257720	0.02172239
C	0.28849443	-2.33690937	-1.70966136
H	0.17511658	-1.59509692	-2.49446485
C	-1.77665255	3.73498931	0.78483258
H	-2.78370833	4.12703668	0.69870739
C	0.37477742	-2.73312072	0.63196318
O	-0.49756968	0.42983089	-1.76458796
H	1.40268218	-3.37757811	3.30447453
C	3.44141493	2.67183949	3.07170313
H	2.56986485	3.13724129	3.54666581
H	3.50405894	1.63438431	3.41893616
H	4.33807080	3.19855740	3.41688328

Table S4. Coordinate file of the DFT optimized structure of metal peroxo intermediate generated in the catalytic cycle of complex **1**.

Cu	-2.117518000000	0.679377000000	-0.202544000000
O	-3.886997000000	2.594638000000	1.124845000000
O	-1.561360000000	-0.002936000000	3.039598000000
N	-1.281959000000	2.494233000000	-0.219672000000
N	-1.396378000000	0.877261000000	1.945522000000
N	-3.323739000000	-0.748527000000	-0.793969000000
N	-3.880669000000	1.481207000000	0.484332000000
C	-0.878699000000	2.987406000000	0.990447000000

C	-4.917659000000	0.698139000000	0.230990000000
C	-5.630510000000	-1.457729000000	-0.877503000000
H	-6.671777000000	-1.279742000000	-0.630161000000
C	-0.992792000000	2.093481000000	2.155043000000
C	-0.383436000000	4.296225000000	1.110491000000
H	-0.070813000000	4.674062000000	2.079110000000
C	-5.240466000000	-2.600413000000	-1.596481000000
H	-5.985836000000	-3.324219000000	-1.912065000000
C	-3.880669000000	-2.795637000000	-1.913596000000
H	-3.554260000000	-3.659975000000	-2.480860000000
C	-0.314774000000	5.108351000000	-0.037179000000
H	0.044286000000	6.130322000000	0.036653000000
C	-1.202598000000	3.261655000000	-1.329906000000
H	-1.538075000000	2.821087000000	-2.262833000000
C	-2.942156000000	-1.840924000000	-1.492160000000
H	-1.882572000000	-1.919679000000	-1.715159000000
C	-0.725428000000	4.584259000000	-1.276117000000
H	-0.700816000000	5.184231000000	-2.179416000000
C	-4.646360000000	-0.529722000000	-0.486579000000
O	-0.644429000000	-0.252096000000	-1.094461000000
H	-5.911440000000	0.992931000000	0.554543000000
H	-0.746163000000	2.490776000000	3.141495000000
H	-1.535662000000	0.485276000000	3.904438000000
O	0.644429000000	0.252096000000	-1.094461000000
Cu	2.117518000000	-0.679377000000	-0.202544000000
N	1.396378000000	-0.877261000000	1.945522000000
N	3.323739000000	0.748527000000	-0.793969000000
N	3.880669000000	-1.481207000000	0.484332000000
N	1.281959000000	-2.494233000000	-0.219672000000
O	1.561360000000	0.002936000000	3.039598000000
C	0.992792000000	-2.093481000000	2.155043000000
C	2.942156000000	1.840924000000	-1.492160000000
C	4.646360000000	0.529722000000	-0.486579000000
O	3.886997000000	-2.594638000000	1.124845000000
C	4.917659000000	-0.698139000000	0.230990000000
C	0.878699000000	-2.987406000000	0.990447000000
C	1.202598000000	-3.261655000000	-1.329906000000
H	1.535662000000	-0.485276000000	3.904438000000
H	0.746163000000	-2.490776000000	3.141495000000
C	3.880669000000	2.795637000000	-1.913596000000
H	1.882572000000	1.919679000000	-1.715159000000
C	5.630510000000	1.457729000000	-0.877503000000
H	5.911440000000	-0.992931000000	0.554543000000
C	0.383436000000	-4.296225000000	1.110491000000
H	1.538075000000	-2.821087000000	-2.262833000000
C	0.725428000000	-4.584259000000	-1.276117000000
C	5.240466000000	2.600413000000	-1.596481000000
H	3.554260000000	3.659975000000	-2.480860000000
H	6.671777000000	1.279742000000	-0.630161000000
H	0.070813000000	-4.674062000000	2.079110000000

C	0.314774000000	-5.108351000000	-0.037179000000
H	0.700816000000	-5.184231000000	-2.179416000000
H	5.985836000000	3.324219000000	-1.912065000000
H	-0.044286000000	-6.130322000000	0.036653000000

Table S5. Coordinate file of the DFT optimized structure of metal peroxo intermediate generated in the catalytic cycle of complex **2**.

Cu	-0.117553000000	0.351219000000	0.466715000000
O	-0.958335000000	3.006129000000	-0.729926000000
H	-0.098516000000	3.162452000000	-0.174617000000
O	1.134320000000	2.811529000000	0.737486000000
N	1.337394000000	-0.861270000000	-0.719522000000
N	1.402094000000	1.543872000000	0.431598000000
N	-1.795240000000	-0.680802000000	0.414613000000
N	-1.313246000000	1.693122000000	-0.468351000000
C	2.569243000000	-0.293471000000	-0.527223000000
C	-2.514901000000	1.284839000000	-0.791201000000
C	-4.010605000000	-0.767278000000	-0.522139000000
H	-4.802013000000	-0.307961000000	-1.103706000000
C	2.561270000000	1.082151000000	0.005685000000
C	-3.538113000000	2.130593000000	-1.493316000000
H	-3.140051000000	3.127539000000	-1.686491000000
H	-3.822957000000	1.675614000000	-2.451141000000
C	3.789391000000	1.955044000000	0.016458000000
H	3.534034000000	2.964920000000	0.342716000000
H	4.236078000000	2.006705000000	-0.983915000000
H	4.545523000000	1.547528000000	0.700801000000
C	3.752894000000	-0.973208000000	-0.870260000000
H	4.720547000000	-0.511617000000	-0.708902000000
C	-4.188148000000	-2.042329000000	0.053000000000
H	-5.122875000000	-2.576147000000	-0.089819000000
C	-3.156388000000	-2.611532000000	0.819874000000
H	-3.270570000000	-3.582085000000	1.289736000000
C	3.660372000000	-2.265284000000	-1.417688000000
H	4.560049000000	-2.809991000000	-1.687676000000
C	1.252909000000	-2.103642000000	-1.240388000000
H	0.255977000000	-2.512759000000	-1.373630000000
C	-1.955696000000	-1.894288000000	0.979758000000
H	-1.120109000000	-2.259084000000	1.570611000000
C	2.392688000000	-2.843069000000	-1.609045000000
H	2.283076000000	-3.835425000000	-2.033151000000
C	-2.796335000000	-0.093461000000	-0.320407000000
O	0.394333000000	-0.584130000000	2.099831000000
O	1.787599000000	-0.698235000000	2.449153000000
H	1.905416000000	-0.038795000000	3.180322000000
H	-4.446426000000	2.226589000000	-0.885256000000

Table S6. Coordinate file of the DFT optimized structure of metal peroxo intermediate generated in the catalytic cycle of complex **3**.

Cu	-0.034465000000	-0.229676000000	0.487498000000
O	1.220912000000	-2.742310000000	-0.642057000000
H	0.381284000000	-3.018377000000	-0.100395000000
O	-0.902060000000	-2.850122000000	0.782418000000
N	-1.643847000000	0.728342000000	-0.738881000000
N	-1.354196000000	-1.640942000000	0.454147000000
N	1.465963000000	1.046052000000	0.430450000000
N	1.358280000000	-1.382635000000	-0.411808000000
C	-2.776468000000	-0.017991000000	-0.547619000000
C	2.484559000000	-0.801493000000	-0.745280000000
C	3.646906000000	1.462857000000	-0.495318000000
H	4.505083000000	1.127141000000	-1.065992000000
C	-2.564790000000	-1.367801000000	0.009198000000
C	3.631970000000	-1.521202000000	-1.406223000000
H	3.228051000000	-2.339907000000	-2.008912000000
H	4.154458000000	-0.835610000000	-2.083821000000
C	-3.645517000000	-2.417672000000	0.022585000000
H	-3.242626000000	-3.371848000000	0.367109000000
H	-4.067742000000	-2.551201000000	-0.980818000000
H	-4.462692000000	-2.120655000000	0.693524000000
C	-4.046189000000	0.466758000000	-0.913318000000
H	-4.933669000000	-0.134852000000	-0.752333000000
C	3.620715000000	2.756674000000	0.064404000000
H	4.463056000000	3.426460000000	-0.080245000000
C	2.507837000000	3.169408000000	0.817527000000
H	2.466691000000	4.151791000000	1.274689000000
C	-4.146077000000	1.748620000000	-1.482916000000
H	-5.115299000000	2.144689000000	-1.770617000000
C	-1.744431000000	1.960249000000	-1.281212000000
H	-0.820244000000	2.514819000000	-1.412878000000
C	1.431787000000	2.276602000000	0.979840000000
H	0.544828000000	2.514679000000	1.560461000000
C	-2.979497000000	2.510439000000	-1.673272000000
H	-3.018006000000	3.500803000000	-2.114145000000
C	2.550467000000	0.610284000000	-0.293270000000
O	-0.709220000000	0.648700000000	2.090750000000
O	-2.108878000000	0.552099000000	2.421654000000
H	-2.133794000000	-0.105310000000	3.163553000000
C	4.630721000000	-2.102467000000	-0.363488000000
H	5.444879000000	-2.615527000000	-0.886242000000
H	5.070682000000	-1.318314000000	0.264506000000
H	4.133175000000	-2.830430000000	0.285828000000

Table S7. TON calculated for complexes **1**, **2** and **3** for chemically driven water oxidation catalytic activity using Cerium ammonium nitrate (CAN) as the primary chemical oxidant

Complex	**TON (s^{-1})**
1	0.011
2	0.017
3	0.019